This is a peer-reviewed, accepted author manuscript of the following research article:
Azarbakht, A., Ebrahimian, H., Jalayer, F., & Douglas, J. (2022). Variations in hazard during earthquake sequences between 1995 and 2018 in western Greece as evaluated by a Bayesian ETAS model. Geophysical Journal International.
https://doi.org/10.1093/gji/ggac177

Variations in hazard during earthquake sequences between 1995 and 2018 in western Greece as evaluated by a Bayesian ETAS model

Authors details:

Alireza Azarbakht[1,*] https://orcid.org/0000-0003-3627-652X, Email: alireza.azarbakht@strath.ac.uk

Hossein Ebrahimian[2] https://orcid.org/0000-0002-4032-9084, Email: ebrahimian.hossein@unina.it

Fatemeh Jalayer[2] https://orcid.org/0000-0002-7580-8309, Email: fatemeh.jalayer@unina.it

John Douglas[1] https://orcid.org/0000-0003-3822-0060, Email: john.douglas@strath.ac.uk

[1]University of Strathclyde
Department of Civil and Environmental Engineering
James Weir Building
75 Montrose Street
Glasgow
G1 1XJ
United Kingdom

[2]University of Naples Federico II
Department of Structures for Engineering and Architecture
Via Claudio 21
Naples
80125
Italy

* Corresponding author: Alireza Azarbakht, Email: alireza.azarbakht@strath.ac.uk

Page heading: Variations in hazard during earthquake sequences

SUMMARY

Forecasting the spatio-temporal occurrence of events is at the core of Operational Earthquake Forecasting, which is of great interest for risk management, particularly during ongoing seismic sequences. Epidemic type aftershock sequence (ETAS) models are powerful tools to estimate the occurrence of events during earthquake sequences. In this context, a robust seismicity forecasting framework based on Bayesian-inference has been adapted to the Patras and Aegio region in western Greece (one of the most seismically active parts of Mediterranean), and an incremental adaptive algorithm is introduced to train the priors for ETAS model parameters. The seismicity forecasting is capable of accounting for uncertainty in the model parameters as well as variations in the sequence of events that may happen during the forecasting interval. Six seismic sequences between 1995 and 2018 were selected with mainshock moment magnitudes $M_w \geq 6.0$. The ETAS model was adapted for each seismic sequence. The number of forecasted events with Mw≥4.5 and their spatial distribution was retrospectively compared with the as-recorded earthquake catalogue, confirming a good agreement between the forecasts and observations. The results show that the adapted model can be employed immediately after a severe mainshock to statistically predict potentially damaging earthquakes during the ongoing seismic sequence. The seismicity forecasts were translated to short-term daily exceedance rates for different thresholds of peak ground acceleration. The results reveal that the seismic hazard increased by up to 33 times in the case of the damaging 1995 Mw 6.5 earthquake in the city of Aegio. However, the results confirmed that in all six studied sequences, the increased seismic hazard decayed rapidly during the two days after the mainshock, and remained relatively high in the following days (roughly ten times the long-term time-independent hazard).

Keywords

Earthquake interaction; forecasting and prediction; Earthquake hazards; Computational seismology.

1 INTRODUCTION

Estimating time-dependent probabilities of occurrence of potentially damaging earthquakes are at the heart of Operational Earthquake Forecasting (OEF) (Jordan et al. 2014). The output of OEF is often given in terms of probability changes due to time-dependent (over the order of days to months) seismicity. These probabilities can be used by emergency managers to communicate with the public

(Jordan and Jones 2010; Goltz 2015; Roeloffs and Goltz 2017; McBride et al. 2020; Field and Minler 2018; Douglas and Azarbakht 2021; Azarbakht et al. 2021). Epidemic type aftershock sequence (ETAS) is a family of spatio-temporal point process models providing estimates of the time-dependent seismicity over a predefined aftershock zone (Ogata 1988; Ogata 1998). ETAS models show promising results in forecasting aftershocks and perform quite well in prospectively forecasting the seismicity within various operational frameworks (e.g. Marzocchi and Lombardi 2009; Zhuang 2011; Marzocchi and Murru 2012; Marzocchi et al. 2014; Ebrahimian and Jalayer 2017; Cattania et al. 2018; Kourouklas et al. 2020). According to the study by Console et al. (2007), the ETAS model is the best model for describing short-term seismicity (see also Zhuang et al. 2011). ETAS is an epidemic stochastic point process that considers every event as a potential trigger for subsequent events, thus, generalising the modified Omori (MO) aftershock decay model (Zhang and Shcherbakov 2016, see also Utsu 1961; Utsu and Ogata 1995). In other words, the ETAS model is capable of accounting for the triggering effects of all events in the earthquake catalogue prior to the considered forecasting time interval. It is worth emphasising that an ETAS model's time-dependent seismicity rate can be transformed into a time-dependent hazard model via Probabilistic Seismic Hazard Analysis (PSHA, Cornell 1968; McGuire 1995), as is discussed in the last section of this article.

In the present article, a simulation-based framework is employed for both Bayesian updating of spatio-temporal ETAS model parameters as well as to obtain robust estimates of the spatial distribution of events in a prescribed forecasting time interval after a mainshock (see Ebrahimian and Jalayer 2017). The term "robust" here relates to the concept of *robust reliability* (Papadimitriou et al. 2001, Beck and Au 2002), which implies both the uncertainties in ETAS model parameters and those related to the occurrence of events in the forecasting interval are considered. The Bayesian inference framework allows the model parameters to be updated with time since the mainshock. In other words, the model adapts itself to the new conditions that the seismicity variations dictate. To clarify, the robust forecasting terminology implies that several sets of model parameters are used through the simulation algorithm instead of using a set of constant model parameters, as is discussed in the methodology section (see also Ebrahimian and Jalayer 2017). A Markov Chain Monte Carlo (MCMC) simulation scheme (Ebrahimian and Jalayer 2017; Omi et al. 2015; Papadimitriou et al. 2001) is used to sample directly from the conditional posterior probability distributions of the ETAS model parameters. This forecasting framework accounts for two sources of uncertainty: (1) the uncertainty in the ETAS model parameters conditioned on the available catalogue of observed events prior to the forecasting interval's origin time, and (2) the uncertainty in the simulated sequence of events during the forecasting time interval. The outcomes of this framework are in terms of the spatial distribution of the forecasted events and consequently the mean and confidence interval for the estimated number of events, corresponding to a given forecasting interval. The latter results are then converted to seismic hazard estimates, here short-term (hours to weeks) probabilities of exceeding different levels of peak ground acceleration (*PGA*), which is chosen as the ground-motion intensity measure because of its common use in seismic hazard mapping.

This article aims to demonstrate the feasibility of the proposed Bayesian framework and retrospectively study the aftershock seismicity and hazard forecasts in the Patras and Aegio region in western Greece. This area is chosen for this study since it is in one of Europe's highest seismicity regions with numerous recent earthquake sequences, and it is a testbed of the TURNkey project[1].

The seismicity characteristics of the region and the available literature are reviewed in the next section. Following this, the input data and the selected earthquake sequences are discussed. Then, following a brief description of the employed forecasting framework, the retrospective spatio-temporal forecasting of seismicity in the region is studied using this methodology. Subsequently, a daily PSHA is presented by combining the seismicity forecasts with three ground-motion models. The article ends with some brief conclusions.

2 REGION OF STUDY

The geodynamic characteristics of the study region are comprehensively discussed in Karakostas et al. (2020). The study area in western Greece includes the third-largest (in terms of population) city in Greece, Patras, with many essential infrastructures, including a large port. There are also many public

[1] Towards more Earthquake-resilient Urban Societies through a Multi-sensor-based Information System enabling Earthquake Forecasting, Early Warning and Rapid Response actions (https://earthquake-turnkey.eu/)

buildings, schools and heritage monuments. Additionally, the Rio–Antirrio bridge crosses the Gulf of Corinth near Patras. This is one of the world's longest multi-span cable-stayed bridges and the longest of the fully suspended type. The town of Aegio is also located in the region, which is famous for a topographic plateau across a major fault (the cause of the destructive earthquake on 15 June 1995). There are also two smaller towns, Kalavryta and Lidorikion, in the region. In this section, we briefly summarise the recent literature on seismic hazard and previous earthquake forecasts for this region.

Both time-independent and time-dependent seismic hazards in Greece were investigated in terms of macroseismic intensity by Papaioannou and Papazachos (2000) for 144 cities, towns, and villages. They concluded that the time-dependent seismic hazard results are in good agreement with the observed seismicity during the period 150 to 1995. A detailed areal-source seismic zonation model for shallow earthquakes in the broader Aegean area, containing 113 zones, was proposed by Vamvakaris et al. (2016). This model was based on seismicity and the available seismotectonic and neotectonic information to represent active faulting characteristics. A detailed investigation of catalogue completeness for the recent instrumental period was also conducted. The seismicity parameters, such as Gutenberg-Richter values for the 113 proposed zones, were calculated, and their spatial distribution was also considered. A review of the official seismic hazard maps in Greece was given by Tsapanos (2008).

Spatio-temporal earthquake clustering in the western Corinth gulf was investigated by Karagianni et al. (2013) by considering geological, seismological, and geodetic aspects. The results reveal complicated tectonic behaviour and strong indications that seismicity in the area is not random and forms distinctive clusters. Console et al. (2006) applied various forecasting algorithms to the Greek catalogue for two periods: 1966-1980 and 1981-2002. The forecasting capability was statistically assessed by using the log-likelihood method. Their results revealed that short-term and long-term methods performed much better than time-invariant models. Gospodinov and Rotondi (2006) and Gospodinov et al. (2007) studied the temporal decay in eight Greek aftershock sequences since 1975 using a Restricted ETAS model (RETAS). The RETAS model assumes that only aftershocks of magnitudes bigger than or equal to a given threshold can trigger secondary events. Karakostas et al.

(2014) focused on forecasting, temporally and spatially, the 2013 Mw 5.8 north Aegean seismic sequence. They employed different statistical methods to simulate the aftershock sequence, including an ETAS model with pre-calibrated parameters. Their results indicate a significant Probability Gain (PG) of more than 20 times the background probability during the first days of the considered aftershock sequence. Latoussakis et al. (1991), Latoussakis and Drakatos (1994), and Drakatos and Latoussakis (1996) studied the possibility of forecasting large earthquakes in Greece during different sequences. They used the MO formula and noted its acceptable accuracy. Telesca et al. (2001) analysed the temporal properties of Greek aftershock sequences using the MO model. A physics-based and statistical earthquake forecasting approach was applied by Segou (2016) to the continental rift zone of the Corinth Gulf, by implementing a retrospective forecast of events with magnitudes greater than or equal to 3 for the time period 1995-2013. This study revealed that the joint implementation of physics-based approaches and the statistical ETAS model is beneficial for future OEF systems. Kourouklas et al. (2020) investigated short-term spatio-temporal clustering of Greek seismicity from 2008 to 2018. The employed ETAS model used maximum-likelihood estimation through a simulated annealing approach. The discrepancies between the ETAS model forecasts and the observations were assessed by residual analysis. The model performed well except for the 2008 sequence when five Mw>6 earthquakes occurred. Finally, the short-term seismicity of the central Ionian Islands was studied by Mangira et al. (2020), revealing that the employed ETAS clustering model provides reliable forecasts of the aftershock activity for this region.

To be complementary to the available literature, the current study uses the most recent seismic data for the region from 1995 to 2018, which contains six earthquakes with $M_w \geq 6$, as explained in detail in the next section.

3 INPUT DATA AND SELECTED SEQUENCES

The International Seismological Centre (ISC, last access 2020) earthquake catalogue (Bondár and Storchak 2011; ISC 2020) was used to collect data from the previous three decades in the study region. It was concluded that six severe mainshocks with their triggered aftershock sequences are distinguishable since the catastrophic 1995 Aegio event. It is assumed that these six sequences are sufficient samples to have both a set of consistent and modern instrumental data, and sufficient sequences to study the potential variation in model parameters. The spatial and temporal characteristics of the ISC catalogue for the study area between 1995 and 2018 (including the six seismic sequences A to F) are shown in Figure 1 and Figure 2, respectively. The cumulative number of earthquakes with Mw $\geq$ 3 is also shown in Figure 2, indicating heightened seismicity around the selected sequences. Greek national catalogues were not used here; however, they are identical with the ISC catalogue beyond the magnitude of completeness. In Greece, there are two institutions reporting phases (bulletin data) to ISC: NOA and Aristotle University of Thessaloniki (AUTH). In other words, there is no common national bulletin in Greece, although, since 2007, there is a unified network sharing waveform data with the public. NOA is the official seismic monitoring agency in Greece, which provides the majority of Greek data to ISC. Nevertheless, the ISC reports some small earthquakes (particularly in northern Greece) using AUTH data. Therefore, the ISC catalogue is the most rational choice for the current study.

The selected earthquake sequences are listed in Table 1, covering mainshocks with moment magnitude Mw $\geq$ 6 between 1995 and 2018. The distances between each mainshock’s epicentre and the two studied cities (Patras and Aegio) are also provided in Table 1 (sequences A and C are the closest to Patras and Aegio, including sequence A, which was only 23 km from Aegio). These differences in distance will influence the seismic hazard assessed at the considered locations, as discussed below.

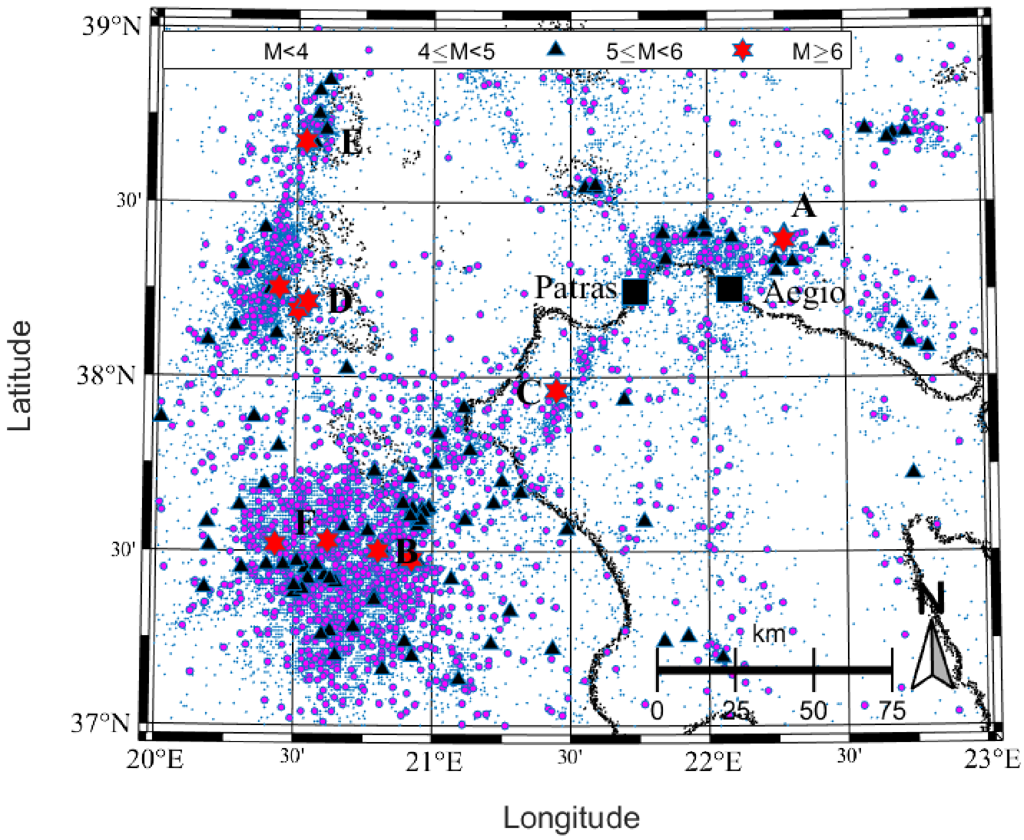

Figure 1. The spatial distribution of the earthquakes between 1995 and 2018 in the study area. The selected seismic sequences are indicated by the capital letters next to the mainshock epicentre (see Table 1).

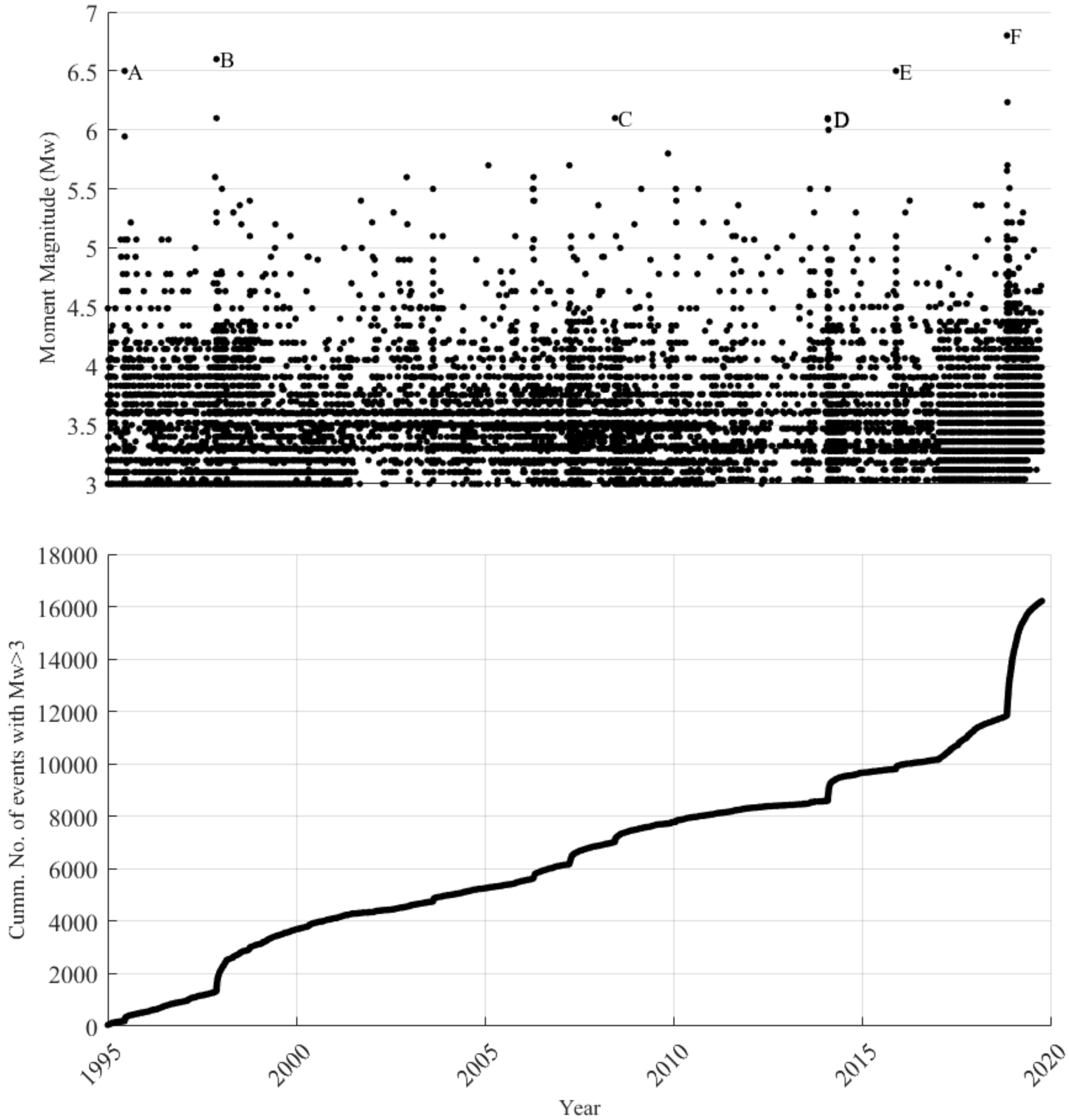

Figure 2. (top): The events with Mw ≥ 3 versus time in the ISC earthquake catalogue between 1995 and 2018 in the study area, including the labelled sequences in Table 1, (bottom): The cumulative number of events with Mw ≥ 3 between 1995 and 2018.

Table 1. The selected sequences between 1995 and 2018 with mainshock magnitude Mw≥6, mainshock occurrence time, and the distances to the cities of Patras and Aegio.

Sequence Label	Lat. (N)	Lon. (E)	Mainshock Magnitude (Mw)	Mainshock Date (dd/mm/yyyy)	Hour:Minute	Distance to Patras (km)	Distance to Aegio (km)
A	38.39	22.28	6.5	15/06/1995	00:15	50	23
B	37.50	20.80	6.6	18/11/1997	13:07	116	140
C	37.96	21.45	6.1	08/06/2008	12:25	40	64
D	38.19	20.51	6.1	26/01/2014	13:55	107	137
E	38.68	20.53	6.5	17/11/2015	07:10	115	143

F	37.53	20.62	6.8	25/10/2018	22:54	126	151

4 METHODOLOGY

Seismicity forecasts over periods of hours/days/weeks are crucial for emergency responders and decision-makers seeking to mitigate risk since there is a high chance of aftershocks during this period. It is clear that forecasting damaging earthquakes have a higher priority than forecasting small events, which is practically impossible. Therefore, this study's focus is to forecast events with magnitudes ≥ 4.5, which is the cut-off magnitude often considered in European seismic hazard studies (Woessner et al., 2015). A robust seismicity forecasting framework (Ebrahimian and Jalayer 2017) has been implemented for this study. By pairing the Bayesian inference with an advanced simulation technique (namely, MCMC) to update the ETAS model parameters, this framework has the unique feature of considering different sources of uncertainty, i.e. the uncertainties in the ETAS model parameters and the generated sequence of events within the forecasting interval (sequences are generated based on samples of the ETAS model parameters).

4.1 The epidemic-type aftershock sequence (ETAS) model

The ETAS model is a marked spatio-temporal point process (Daley and Vere-Jones 2003), where a seismic sequence is treated as a point process of inter-event time and epicentres. The magnitude of each event is an additional observed variable characterizing the point process to become marked. Let the aftershock zone be defined as set **A** in the Cartesian space. The conditional rate of occurrence of earthquakes at time t with magnitude ≥ m in the cell unit centred at the Cartesian coordinate $(x, y) \in$ **A** based on the ETAS model is denoted as $\lambda_{\mathrm{ETAS}}(t, x, y, m|\boldsymbol{\theta}, \mathbf{seq}_t, M_l)$. The rate λ_{ETAS} is conditioned on: (1) the vector of ETAS model parameters $\boldsymbol{\theta}$ (defined subsequently); (2) the observation history up to time t, which expresses the influence of past events $\mathbf{seq}_t = \{(t_j, x_j, y_j, m_j), t_j < t, M_j \geq M_l\}$ where t_j is the arrival time for the j^{th} event (with $t_j < t$) with magnitude m_j and location $(x_j, y_j) \in$ **A**; and (3) the lower cut-off magnitude M_l. The conditional rate λ_{ETAS} can be computed as follows:

$$\lambda_{\mathrm{ETAS}}(t, x, y, m|\boldsymbol{\theta}, \mathbf{seq}_t, M_l) = e^{-\beta(m-M_l)} \sum_{t_j<t}\left[K\, e^{\beta(m_j-M_l)} \frac{K_t}{(t-t_j+c)^p} \frac{K_R}{({r_j}^2+d^2)^q}\right] \quad \text{(Eq. 1)}$$

In Equation (1), the background seismicity rate is not considered; this issue will be discussed in the subsequent section. The vector of ETAS model parameters is defined as $\boldsymbol{\theta} = [K, K_t, K_R, \beta, c, p, d, q]$. Parameter β is related to the Gutenberg-Richter relation; parameters c and p are similar to those of the MO's Law defining the decay in time; d and q characterise the spatial distribution of the triggered events; r_j is the distance between the location (x, y) and the epicentre of the j^{th} event (x_j, y_j). The parameter K requires calibration for each forecasting interval and is discussed in the subsequent section. The parameter K_t is computed so that the time-dependent term $K_t/(t - t_j + c)^p$ over infinite time will, in the limit, be equal to unity (see Ebrahimian and Jalayer 2017 and Lippiello et al. 2012 and 2014), which results in $K_t = (P - 1) \cdot c^{(p-1)}$. Finally, the parameter K_R is normalised such that integrating the spatial term over infinite space will also, in the limit, be equal to unity (see Ebrahimian and Jalayer 2017 and Lippiello et al. 2012 and 2014) resulting in $K_r = \frac{(q-1)}{\pi} \cdot d^{2(q-1)}$. In the ETAS model (Equation 1), the term $Ke^{\alpha(M_j - M_l)}$ is called the productivity function and the coefficient α shows the efficiency of an event in generating aftershock activity (dimension of magnitude^{-1}). It is assumed herein that $\alpha = \beta$ (for more details, see the parameter α in Ogata and Zhuang 2006). Hence, in summary, only five model parameters (i.e., $[\beta, c, p, d, q]$) are used in the MCMC updating framework. The other three parameters ($[K, K_t, K_R]$) are calculated as described above (for more details, see Ebrahimian and Jalayer 2017). It is noted that the generated sample through the MCMC algorithm is rejected if any of the following conditions hold: (1) any value of the vector $[\beta, c, p, d, q]$ is negative, (2) $p \leq 1$, or (3) $q \leq 1$ (the latter two conditions are described in Ebrahimian and Jalayer 2017). It is also worth mentioning that the focus of the current study is forecasting over a short time interval (e.g. one day), otherwise, the β coefficient in the productivity function may cause the population to explode when simulating for a relatively long time period.

To clarify, the assumption of equality between the two parameters α and β is a commonly adopted constraint (see e.g. Seif et al. 2017; Zhang et al. 2018; Papadopoulos et al. 2021). When α is considered to be a free parameter in the ETAS model (i.e. the model parameters become $[\alpha, \beta, c, p, d, q]$), past studies based on maximum-likelihood estimation (e.g. Marzocchi and Lombardi

2009) or Bayesian parameter estimation (Ebrahimian and Jalayer 2021) showed that $\alpha < \beta$. In particular, the parameter α determines the magnitude dependence of the trigger potential, which is crucial in identifying the underlying triggering mechanism and for forecasting ongoing earthquake sequences (Hainzl et al. 2013). The constraint $\alpha = \beta$ implies self-similarity of the triggering events (i.e. the number of triggered events is proportional to the rupture area of the triggering earthquake, see Papadopoulos et al. 2021). Moreover, it is shown that α might be significantly underestimated (low value of α) due to the incompleteness of the aftershock catalogue and missing data at the early stages of an ongoing seismic sequence (Seif et al. 2017). This issue may be critical in terms of providing operational forecasts in the immediate aftermath of a large earthquake. Moreover, in the study region (Greece), where the recorded catalogue is not rich in low-magnitude events (see Section 4.3), this consideration might underestimate the parameter α. There are also other issues that have a significant influence on the estimation of the parameter α including anisotropic aftershock distribution (Hainzl et al. 2008), potential time-dependent (nonstationary) background rate and transient aseismic forcing (Hainzl et al. 2013, who show that the majority of earthquake clusters in California are compatible with $\alpha = \beta$). Therefore, to avoid these potential biases, we have assumed $\alpha = \beta$ in the current study.

4.2 Estimation for the number of aftershocks

With reference to Equation (1), let $\lambda_{\text{ETAS}}(t, x, y, m|\boldsymbol{\theta}, \mathbf{seq}, M_l)$ be the conditional intensity representing the ETAS rate of occurrence of events in the forecasting interval [T_{start}, T_{end}] at time t (elapsed after the main event, or even any arbitrary time reference) with the time of origin at T_o. The observation history **seq** is the sequence of N_o events (including the mainshock and the sequence of aftershocks) that took place before the forecasting interval, i.e., in the interval [T_o, T_{start}). This can be expressed as $\mathbf{seq} = \{(t_i, x_i, y_i, m_i), T_o \le t_i < T_{start}, m_i \ge M_l, i = 1{:}N_o\}$. The number of events at the centre point of a given cell centred at (x, y) with magnitude $\geq$ m in the forecasting interval [T_{start}, T_{end}], denoted as $(x, y, m|\mathbf{seq}, M_l)$, can be estimated by:

$$N(x, y, m|\mathbf{seq}, M_l) = N_b(x, y, m|M_l) + \int_{T_{start}}^{T_{end}} \lambda_{\text{ETAS}}(t, x, y, m|\mathbf{seq}, M_l)\, \mathrm{d}t \qquad \text{(Eq. 2)}$$

where $N_b(x, y, m|M_l)$ is a constant representing the area's background seismicity. It is equal to the time-invariant background spatial seismicity rate for magnitudes > m multiplied by the time interval $(T_{end} - T_{start})$. To clarify, the number of events in the whole cell can be calculated by multiplying N by the area of the cell. Given a realisation of $\boldsymbol{\theta}$ as the vector of ETAS model parameters, parameter K (of the vector $\boldsymbol{\theta}$) is calibrated such that the number of events with magnitude $\geq M_l$ taking place in the time interval $[T_o, T_{start})$, over the whole aftershock zone is equal to N_o (see Ebrahimian and Jalayer 2017 for more details). Moreover, one can calculate a plausible value for the rate of occurrence denoted as $\lambda_{\mathrm{ETAS}}(t, x, y, m|\boldsymbol{\theta}, \mathbf{seq}, M_l)$, as shown in Equation (1). A robust estimate (Ebrahimian and Jalayer 2017) of the average number of events in the cell centred at (x, y) with a magnitude $\geq m$ in the forecasting interval $[T_{start}, T_{end}]$, denoted as $\mathbb{E}[N(x, y, m|\mathbf{seq}, M_l)]$, can be calculated over the domain of the model parameters $\Omega_{\boldsymbol{\theta}}$:

$$\mathbb{E}[N(x, y, m|\mathbf{seq}, M_l)] = N_b(x, y, m|M_l) + \int_{\Omega_{\boldsymbol{\theta}}} \left(\int_{T_{start}}^{T_{end}} \lambda_{\mathrm{ETAS}}(t, x, y, m|\mathbf{seq}, M_l)\, \mathrm{d}t \right) p(\boldsymbol{\theta}|\mathbf{seq}, M_l) \mathrm{d}\boldsymbol{\theta} \quad \text{(Eq. 3)}$$

where $\mathbb{E}[\cdot]$ denotes the expectation, and $p(\boldsymbol{\theta}|\mathbf{seq}, M_l)$ is the conditional posterior probability density function (PDF) for $\boldsymbol{\theta}$ given the $\mathbf{seq}$ and the lower cut-off magnitude M_l. The PDF $p(\boldsymbol{\theta}|\mathbf{seq}, M_l)$ can be estimated using Bayesian parameter estimation, which is discussed in Appendix 1. Equation (3) accounts for the events that took place before the forecasting interval $[T_o, T_{start})$; however, the triggering effect of the events taking place during the forecasting interval $[T_{start}, T_{end}]$ is expected to play a major role. The robust estimate for the average number of aftershocks (as noted previously) also considers all the plausible sequences of events that can happen during the forecasting time interval (see Ebrahimian and Jalayer 2017 for a comprehensive discussion). To this end, the sequence of events taking place during the forecasting interval (denoted herein as **seqg**), which is unknown at the time of forecasts, is simulated. Let us assume that a plausible **seqg** is defined as the events within the forecasting interval defined as $\mathbf{seqg} = \{(IAT_i, x_i, y_i, m_i), T_{start} \leq t_i \leq T_{end}, m_i \geq M_l\}$, where $IAT_i = t_i - t_{i-1}$ stands for the inter-arrival time. The robust estimate for the number of aftershocks in Equation (3) should also consider all the plausible sequences of events **seqg** (i.e., the domain $\Omega_{\mathbf{seqg}}$) that can happen during the forecasting time interval, as follows:

$$\mathbb{E}[N(x,y,m|\mathbf{seq},M_l)] = N_b(x,y,m|M_l) + \int_{\Omega_{\boldsymbol{\theta}}}\left[\int_{\Omega_{\mathbf{seqg}}}\left(\int_{T_{start}}^{T_{end}} \lambda_{\text{ETAS}}(t,x,y,m|\mathbf{seqg},\boldsymbol{\theta},\mathbf{seq},M_l)\,\mathrm{d}t\right) p(\mathbf{seqg}|\boldsymbol{\theta},\mathbf{seq},M_l)\mathrm{d}\mathbf{seqg}\right] p(\boldsymbol{\theta}|\mathbf{seq},M_l)\mathrm{d}\boldsymbol{\theta}$$

(Eq. 4)

where $p(\mathbf{seqg}|\boldsymbol{\theta},\mathbf{seq},M_l)$ is the PDF for the generated sequence **seqg** given that $\boldsymbol{\theta}$ and **seq** are known and $\lambda_{\text{ETAS}}(t,x,y,m|\mathbf{seqg},\boldsymbol{\theta},\mathbf{seq},M_l)$ is the space-time clustering ETAS model considering also the sequence of events taking place within the forecasting interval. The robust estimation in Equation (4) implies that a set of possible model parameters is used to estimate the conditional number of events $N(x,y,m|\mathbf{seq},M_l)$ rather than a single set of model parameters.

The proposed algorithm is demonstrated for six independent seismic sequences in the region (see Section 5). The employed algorithm is shown to successfully forecast aftershocks in all the six considered sequences. The conditional estimation of *N* (see Equation 4) can be used further for short-term time-dependent PSHA. The 2013 European Seismic Hazard Model (ESHM13) (Giardini et al. 2013; Woessner et al. 2015) has been used in the current study to define the background seismicity in Equation (2) to Equation (4). The Kernel-smoothed stochastic rate model considering seismicity and fault moment release (SEIFA-model) has been employed to define each cell's background seismicity rate in the aftershock zone (Woessner et al. 2015).

4.3 The incremental adaptive training algorithm to obtain priors for the ETAS model parameters

Defining prior values for the model parameters $\boldsymbol{\theta}$ is a challenging task. In Greece the aftershock sequences are not particularly productive and/or well-reported, i.e., the magnitude of completeness (M_c) varies between 2.7 to 4.5 for different locations and catalogue lengths (see Vamvakaris et al. 2016). This relatively high magnitude of completeness makes defining the prior values even more challenging. It is not reasonable to wait for a long time after a mainshock to obtain a satisfactory catalogue (for the period after the mainshock only) to initiate the forecasting procedure (especially in the context of operational earthquake forecasting). In other words, we would need to wait a long time after a mainshock (in aftershock sequences of low productivity or high magnitude of completeness) so that sufficient events occur to obtain a complete catalogue if we insist on using only the events following a mainshock (sequence-specific). To clarify, as a solution, it is convenient to "borrow" events from a time window before the mainshock to calibrate the model parameters and consequently update it during the aftershock sequence. Therefore, an *incremental adaptive training algorithm* has been developed and proposed in this study to estimate a set of reasonable priors for the ETAS model parameters $\boldsymbol{\theta}$ to start the forecast algorithm almost immediately after a mainshock (see Figure 3). It is worth emphasising that the proposed adaptive approach is only used for the first round of the forecasting algorithm. The sequence-specific catalogue (from the mainshock's origin time) is then used for the second round (i.e., the second day in this study) of the forecasting trials and so forth. As shown in Figure 3, the proposed algorithm starts its computations from 'M' months before the forecast interval and chooses several arbitrary subsets of 'E' events with magnitude $\geq M_c$. It is worth mentioning that M_c is sequence-specific and is calculated for each sequence separately. In the case of the first round, where the adaptive algorithm in Figure 3 is employed, if we face a quiescent period before the mainshock, we lengthen the catalogue prior to the mainshock to obtain sufficient data to calibrate the prior parameters of the ETAS model. Additionally, in the case of the second round and so forth, we may face a lack of data in the catalogue after the mainshock for calculation of the magnitude of completeness. This lack of data may be due to low productivity in a specific sequence or the aftershock waves being hidden in the seismic waves of the larger events (Lippiello et al. 2016 and 2019). In this case, we move the catalogue origin time T_o back a couple of days before the mainshock, with the aim of having a catalogue that is sufficient to calculate M_c.

Normally-distributed prior model parameters (mean values of b=1, c=0.03, p=1, d=1, q=1.5, all with standard deviation ($\boldsymbol{\sigma}$) equal to 0.3, and $\beta = b \cdot \ln 10$) are used for the first subset of the adaptive incremental algorithm, and the MCMC algorithm is used to update these model parameters based on the first subset catalogue. As an example, the prior and posterior distributions of the 'c' model parameter are shown in Figure 4. As seen in Figure 4, sample posterior intervals are simulated by the MCMC algorithm, and consequently, a normal distribution is fitted to the posterior numerical histograms. In other words, an advantage of the currently employed model is that the model parameters are not constant during a seismic sequence, which is in contrast with ETAS models based on the maximum-likelihood approach.

Subsequently, the previous subset's posterior distributions are used as the prior distributions for the next subset. This procedure repeats until we reach the last subset, which ends before the starting time of the forecast (T_{start}). Each subset is also checked so that it covers at least 'D' days of the catalogue, i.e. if 'E' events happen in less than 'D' days, we increase the subset's time window to cover at least 'D' days.

This proposed algorithm ensures that the final prior distributions for the ETAS model parameters have been trained based on the previous 'M' months catalogue. For example, for Sequence F (see Table 1), the employed catalogue goes back a year before the mainshock (27-1-2018 to 25-10-2018). Hence, as seen in Table 2, we start from 27 January 2018 until the date which provides subsets of at least 50 events with magnitude $\geq M_c$ (equal to 4.1 in this case based on the approach of Wiemer 2001) and covers at least a minimum duration of 30 days. The minimum of 50 events guarantees the proper numerical MCMC updating of the ETAS model parameters (this was empirically verified by the authors); nevertheless, considering a minimum value for D (equal to 30 days herein) will also provide a trade-off between the number of events and the time span in which they took place. The first row in Table 2 indicates that the first subset begins on 27 January 2018 and ends on 14 March 2018, which contains 71 events with $M\geq4.1$. These events were primarily used in the MCMC Bayesian updating algorithm to update the prior model parameters. The updated five (mean) model parameters are also provided in the first row of Table 2. The first row of Table 2 is used as prior information (the mean value, the corresponding $\boldsymbol{\sigma}$ and the normal distribution assumption) for the second row. This procedure was repeated until the last row in Table 2, which is before the forecasting date, i.e. at 00:00 UTC on 26 October 2018 (almost one hour after the mainshock of Sequence F). The proposed incremental adaptive training of the ETAS model parameters needs only the MCMC algorithm to update the ETAS model parameters (subsets 1 to 6 in Table 2). The seismicity forecasting is only performed for the last row in Table 2 (subset 6 in Table 2) in order to provide the spatio-temporal distribution of earthquakes in the forecasting interval of interest, as discussed in the next section.

The adaptive training of the ETAS model parameters provides the opportunity to initiate earthquake forecasting almost immediately after the occurrence of a mainshock, especially in regions with aftershock sequences of low productivity. This is a key forecasting constraint in many high seismicity regions such as Greece in the first (golden) hours after a severe mainshock, during which the forecasting results are of utmost importance for first responders. The possibility of earthquake forecasting immediately after a severe mainshock is of great interest to researchers (e.g. Lippiello et al. 2016 and 2019). The proposed incremental adaptive training algorithm also provides a rational framework to continuously update the prior ETAS model parameters used in an OEF engine on a regular basis. A potential OEF framework may use the last set of updated parameters, when a magnitude greater than a pre-defined threshold occurs, which can potentially define the mainshock of interest. In this context, there is no need to consider a very long sequence (e.g., the whole 419 events in Table 2), which thus overcomes the burden of summing up the triggering properties of all the events when providing early forecasts. Moreover, there is no need to consider the origin time of the sequence if the mainshock is not preceded by foreshocks.

Table 2. The incremental adaptive training of the ETAS model parameters for sequence F (see Table 1).

Number of subsets	Start date (dd-mm-yyyy)	End date (dd-mm-yyyy)	No. of events with $M \geq M_c$	β	c	d	p	q
1	27-01-2018	14-03-2018	71	1.681	0.044	1.014	1.803	1.207
2	17-03-2018	23-04-2018	70	1.679	0.048	1.014	2.050	1.224
3	24-04-2018	17-06-2018	70	1.681	0.054	1.012	2.172	1.230
4	17-06-2018	06-08-2018	70	1.682	0.058	1.010	2.443	1.225
5	06-08-2018	01-10-2018	70	1.682	0.064	1.009	2.535	1.226
6	01-10-2018	25-10-2018	68	1.682	0.065	1.010	2.556	1.227

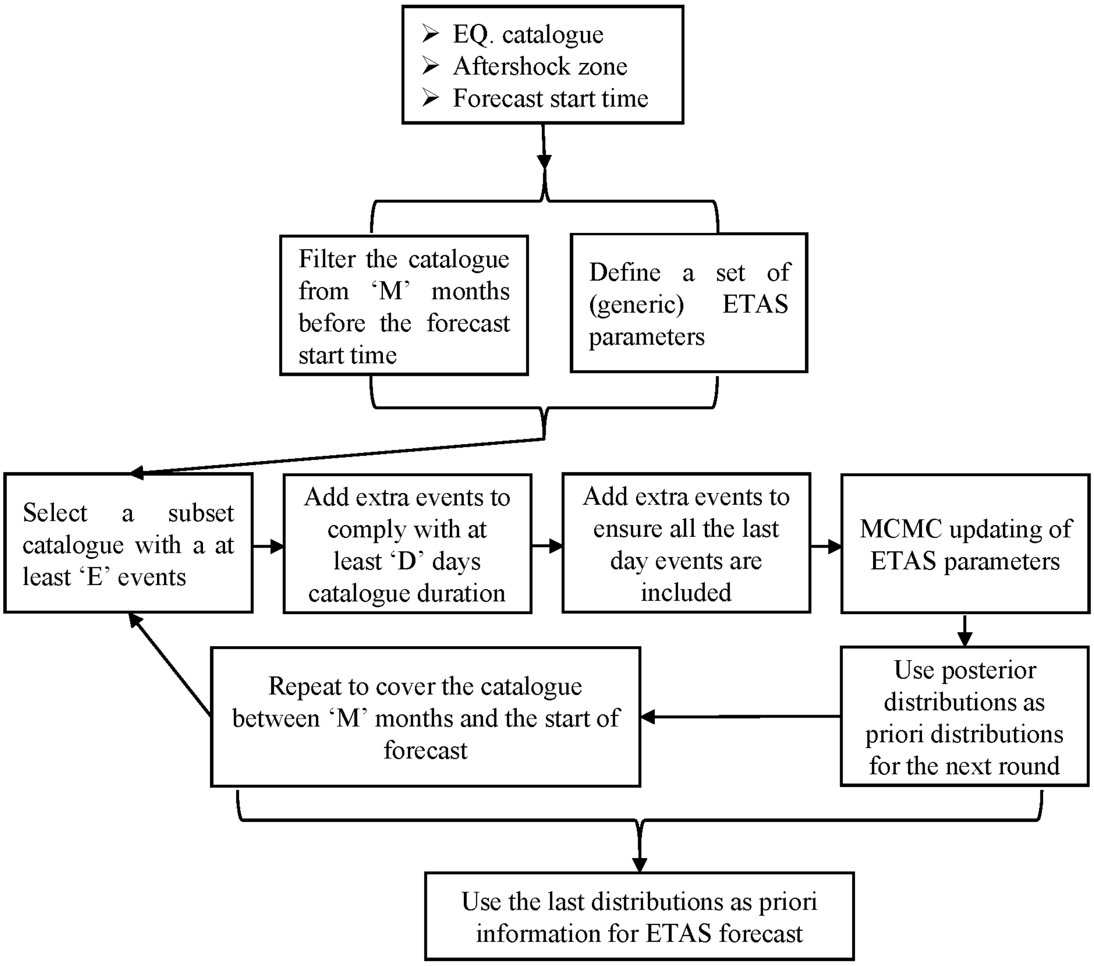

Figure 3. The flowchart of the incremental adaptive training algorithm to obtain the ETAS prior model parameters.

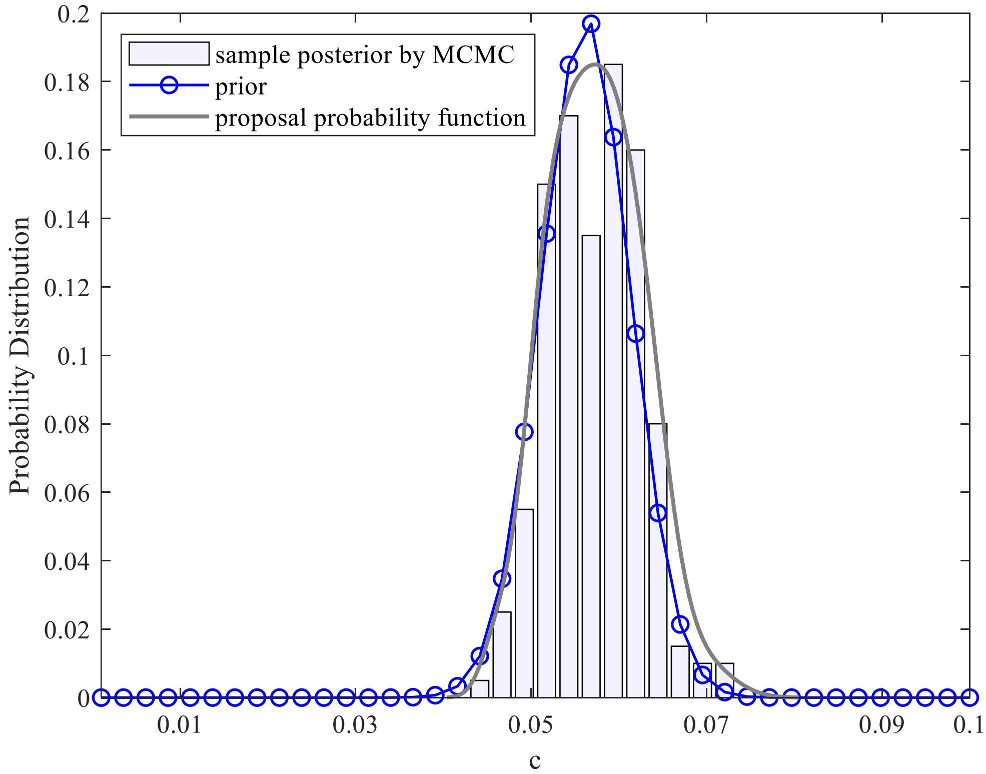

Figure 4. The MCMC updating for the example of the ‘c’ model parameter, showing the prior and posterior distributions.

We summarize the proposed methodology’s steps as follows:

1- Use the incremental adaptive training methodology to obtain prior ETAS model parameters before a mainshock. This set of model parameters is used for the first forecasting attempt after a mainshock.

2- Use the sequence-specific catalogue (between the mainshock’s origin time and the start of the forecasting interval) to obtain the ETAS model parameters for the second forecasting trial and so forth. If the catalogue is not sufficient to estimate the magnitude of completeness, then the catalogue is extended by days/months before the mainshock to obtain sufficient data.

3- To estimate the ETAS model parameters conditioned on the events that have already taken place in the ongoing seismic sequence and before the beginning of the forecasting interval, an MCMC simulation scheme is used to sample directly from the conditional posterior probability distribution for ETAS model parameters. This ETAS model parameter updating is applied to the selected catalogue (from either Step 1 or Step 2 above).

4- Perform many (200 in our study) sequence simulations based on the generated plausible sequences of events that may occur during the forecasting interval (the real sequence is unknown at the time of forecasting).

5- Use Equation (4) to estimate the spatial distribution of the forecasted events and consequently the estimated number of events corresponding to a given forecasting interval with their confidence intervals. The background seismicity can also be included.

6- Employ Equation (6) (see Section 6) to convert forecasted seismicity results into time-dependent seismic hazard estimates.

5 SEISMICITY FORECASTING RESULTS

The study area in Figure 2 is defined between 20-23E and 37-39N and is meshed with a grid size of 0.05×0.05 degrees, which is the same grid size as ESHM13 (Woessner et al. 2015). This choice facilitates the implementation of the seismicity results in the PSHA. This area is the same as in previous studies on these earthquake sequences (e.g. Karakostas et al., 2020). The forecast interval is defined as one day (24 hours), and T_{start} is set at 00:00 UTC. Starting with the most recent mainshock (i.e., sequence F), T_{start} is almost one hour after the mainshock. Sequence F's mainshock had a magnitude Mw of 6.8 and occurred at 37.53N and 20.62E, which is near the southwest corner of the considered aftershock zone (Figure 5, see also Figure 2 and Table 1). It is worth mentioning that ESHM13 (Giardini et al. 2013; Woessner et al. 2015) has been used throughout this paper to define the background seismicity as an input to the ETAS model.

The forecasted short-term spatial distribution of seismicity in terms of the mean plus 2**σ** (98% confidence interval) in the study area is shown in Figure 5, for a forecast interval of one day (24 hours) following T_{start} of 00:00 UTC on 26 October 2018. The observed earthquakes of interest that occurred within the corresponding forecasting interval are also illustrated as coloured dots (distinguished by magnitude). The colour bar in Figure 5 indicates the forecasted number of occurrences (per forecast time interval and per km^2) of events with a magnitude ≥ M_l (we set M_l=M_c=4.1 in this case). M_c is calculated (Wiemer 2001) based on the sequence of events (see **seq** in

Equation 2), which contains 68 observed data from 1-10-2018 to 25-10-2018 (see the last row in Table 2), and eight aftershocks occurred during the 66 minutes between the mainshock time (22:54 UTC) and T_{start} (00:00 UTC). Only eight aftershocks with $M \geq M_c$ took place after the mainshock up to T_{start}; hence, as explained in the previous section, we used the catalogue before the mainshock origin time (see the last row in Table 2) to overcome this shortcoming and to incrementally obtain the model parameters' prior values.

As shown in Figure 5, higher seismicity is forecasted at the closest distances to the mainshock's epicentre. The probabilities of exceeding different magnitude thresholds (from 4.5 to 7.5) are shown in Table 3 for all sequences (A to F in Table 1) and the first forecasting day following the given mainshocks. The upper limit for the magnitude is assumed to be 7.5 since the maximum magnitude in ESHM13 (Giardini et al. 2013; Woessner et al. 2015) for all the 14 SEIFA area sources in the study area are between 7.2 and 8.1. It is worth noting that the probabilities shown in Table 3 refer to an event occurring anywhere inside the study area and cannot be interpreted as a forecast of a specific event at a particular location. These probabilities are the integration of forecasted numbers over all cells (covering the whole study region). For example, the probability of having Mw ≥ 4.5 during the first day following a mainshock anywhere in the whole study area is equal to $0.99\overline{9}$ (=1.00) in the case of sequence F. This forecast is reasonable since there are 32 observed events with Mw ≥ 4.5 in this forecasting time interval (Figure 5 and Table 3).

The forecasted number of events, within the aftershock zone, with Mw ≥ 4.5 (which is the minimum magnitude assumed in ESHM13 for seismic hazard calculation) is also shown in Table 3,indicate the forecasted 50th percentile (the median value, equivalent to the logarithmic mean in an arithmetic scale), the 84th percentile (logarithmic mean plus one logarithmic $\boldsymbol{\sigma}$ in an arithmetic scale), and the 98th percentile (logarithmic mean plus two logarithmic $\boldsymbol{\sigma}$ in an arithmetic scale), respectively. The observed number of events with a magnitude greater than 4.5 is also shown in Table 3 for the purpose of comparison. As seen in Table 3, the forecasted numbers of events are in good agreement with the observed data. This is an inherent criterion to intuitively assess the quality of the forecasting algorithm. To study this agreement more, we estimated the seismicity for different forecasting time intervals. Besides, as seen in Table 4, the results (including statistical percentiles) are provided by repeating the current forecasting algorithm for nine different forecasting time intervals, all with the same T_{start} (i.e., 00:00 UTC on 26 October 2018). The distribution of the forecasted number of events shows good agreement with the observed catalogue, as reported in Table 4. Therefore, the 24-hour forecasting time interval is chosen for further investigations; this is also a reasonable time interval for risk management purposes (see also Ebrahimian et al. 2013 and 2014). It is worth mentioning that the forecasted number of events is calculated as a real number, but is shown in Table 4 after rounding to the closest integer value. Therefore, some percentiles for a given time interval become identical in Table 4.

In addition, the N-test (Zechar et al. 2010) was employed to assess the quality of the forecasts. The N-test is intended to measure (in a probabilistic manner) how well the forecasted number of earthquakes matches the observed number of events. According to this test, we fit a Poisson distribution to the forecasted number of events (N_{fore}) with a magnitude greater than a threshold, which is actually the expected number of events in the forecasting interval that we have estimated. Then, we measure if the observed number of events (N_{obs}) with a magnitude greater than a threshold is not located in the tails of the Poisson distribution. To this end, we estimate two probability terms that should be greater than a pre-defined value P_{eff}: as written in Equation (5).

$$P(n \le N_{\text{obs}} | N_{\text{fore}}) = \sum_{n=0}^{N_{\text{obs}}} \frac{(N_{\text{fore}})^n e^{-N_{\text{fore}}}}{n!} > P_{eff}$$

$$P(n \ge N_{\text{obs}} | N_{\text{fore}}) = 1 - P(n \le N_{\text{obs}} - 1 | N_{\text{fore}}) = 1 - \sum_{n=0}^{(N_{\text{obs}}-1)} \frac{(N_{\text{fore}})^n e^{-N_{\text{fore}}}}{n!} > P_{eff} \quad \text{(Eq. 5)}$$

The above expression guaranties that the real case of N_{obs} will not be within the tails of our forecast. It is worth mentioning that the value for P_{eff} is set to 0.025 to reflect the 95% confidence interval. As seen in Table 4, the N-test column has two numbers in each cell, representing the first and second integrals in Equation (5), respectively. The employed N-test confirms that, in all forecast cases, the N_{obs} is not located within the tails of our forecast. However, providing the statistical distribution of

N_{fore} (see Table 4) is more feasible in the sense that instead of assigning a Poisson distribution to the forecasted number of events, it estimates directly the distribution of the forecast and computes its percentiles (i.e., 50th, 16th, 84th, 2nd and 98th). In this way, one can judge how well the forecasted number of earthquakes matches N_{obs}. Besides, as seen in Figures 5 and 6, the spatial distribution of forecasted events are in very good agreement with the observed events, which again demonstrates the accuracy of the employed algorithm.

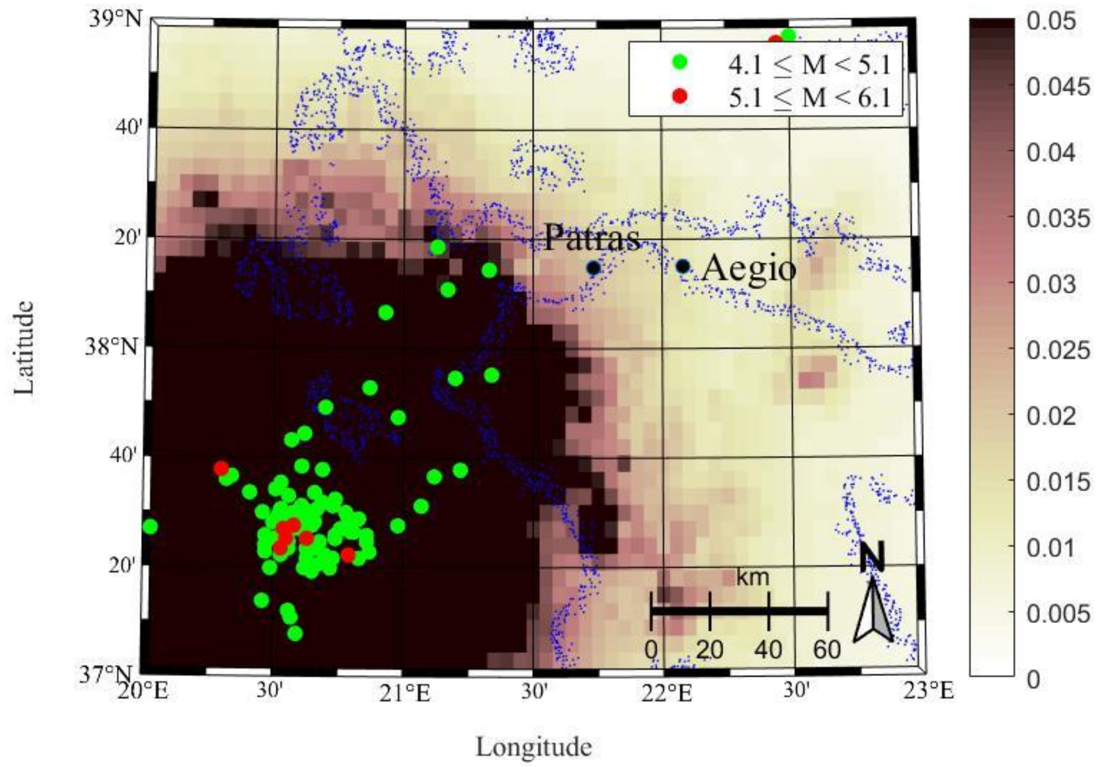

Figure 5. The spatial distribution of the seismicity (the map reports the mean+2**σ** confidence interval, i.e. 98th percentile, for the number of events per km^2) in the aftershock zone for 26 October 2018 (sequence F in Table1). The forecast interval is 24 hours, starting from 00:00 UTC. The probability of having a magnitude greater than or equal to a given magnitude is shown in the figure's bottom-left corner. The forecasted numbers of events with $M \geq 4.5$ are shown in the bottom-right corner. The first, second, and third numbers indicate the 50th, 84th and 98th percentiles. The fourth number (in the parenthesis) indicates the observed number of events.

Table 3. Comparison between the forecasted number of events (and the corresponding statistical distribution) with $M \geq 4.5$ and the observed data in the case of all sequences for the first day after the mainshock. The probabilities of exceeding different magnitude thresholds (from 4.5 to 7.5) over the whole aftershock zone are also shown.

Sequence Label	Number of forecasted events with $M \geq 4.5$			Observed	P(M≥m) over the aftershock zone			
	50th percentile	84th percentile	98th percentile		m=4.5	m=5.5	m=6.5	m=7.5
A	2	2	2	2	.9	.2	.03	.003
B	3	4	4	4	1	.3	.04	.005
C	3	3	4	0	.9	.2	.03	.003
D	1	1	1	4	.6	.1	.01	.001
E	4	5	7	3	1	.5	.1	.02
F	20	24	35	32	1	1	.5	.1

Table 4. Comparison between the forecasted number of events (and the corresponding statistical distribution) with $M \geq 4.5$ and the observed data in the case of sequence F for different forecasting intervals. The forecasting start time, T_{start}, is 00:00 UTC on 26 October 2018.

Forecasting interval	Number of forecasted events with $M \geq 4.5$					Observed	N-test
	2nd percentile	16th percentile	50th percentile	84th percentile	98th percentile		
6 hours	6	7	7	9	12	11	.946, .098
12 hours	9	10	12	15	20	19	.978, .037
1 day	13	16	20	24	35	32	.983, .026
2 days	19	23	30	42	83	39	.953, .064
3 days	23	30	39	57	92	45	.850, .187
4 days	28	36	48	68	109	50	.648, .405
5 days	35	43	61	82	149	61	.483, .567
6 days	39	49	66	93	181	63	.386, .660
7 days	44	54	76	111	189	67	.227, .807

Another advantage of the seismicity forecasting model is its ability to forecast repeatedly during the short duration of most aftershock sequences within an operational framework. Hence, the forecasting model has been run repeatedly every day until seven days following the mainshock (see Table 5). To clarify, we only used the incremental adaptive training of the parameters in the case of forecasting for 26 October (the first row in Table 5), for which **seq** contained 68 events and was defined previously in this section (see the last row of Table 2). However, for the second-day forecast (second row in Table 5) and for subsequent forecasts, we only used the previous day's posterior distribution (the mean value, the corresponding **σ** and the normal distribution) as prior values for the next day.

Additionally, we only used the catalogue starting from the mainshock up to the T_{start}, in the case of forecasting for 27 October and beyond (i.e. the **seq** includes the mainshock and the sequence of the events up to T_{start} of the corresponding date). This change is a rational (as well as an operational) choice; e.g. for daily forecasting starting from 00.00 UTC on 27 October, 25 hours have passed since the mainshock, and we have sufficient events (according to the second column of Table 5, **seq** contains 101 events including the mainshock and the sequence of aftershocks with M>M_c). Thus, there is no longer a need to use the catalogue before the mainshock. However, if we face a lack of data in the catalogue after the mainshock, then, we would move the catalogue's start time back a couple of days before the mainshock, in order to have sufficient data to perform the Bayesian updating. This was not necessary for Sequence 'F', but, this assumption is necessary to make the algorithm versatile. The magnitude of completeness, M_c, in Table 5 is equal to 4.1 (see the third column). The retrospective forecasting results for the number of events with M>4.5 are shown in Table 5, which confirms that the forecasted number of events is in good agreement with the observed data (see the last four columns in Table 5). However, an event with a magnitude (Mw) of 6.2 occurred on 30 October at 02:59 UTC. The ETAS model cannot directly forecast such a severe doublet event. Nevertheless, the forecasted number of earthquakes above the threshold of 4.5 is between 4 and 7, which confirms that the seismicity is still high based on this forecasting model. As seen in Table 5, the employed N-test results also confirm that, in all cases, the N_{obs} is not located within the tails of our forecast.

Table 5. The variation of the model parameters **θ** and seismicity forecasting results for seven days following the mainshock for sequence F (Table 1). The forecasting time interval is equal to 24 hours (1 day) for all seven days with T_{start} = 00:00 UTC at the corresponding date.

Forecast date (dd-mm)	No. of events after the mainshock ($M \geq M_c$)	Mc	β		c		p		d		q		Number of forecasted events with $M \geq 4.5$			Observed	N-test
			median	σ	median	σ	median	σ	median	σ	median	σ	Median	Median+1σ	Median+2σ		
26-10	8 (+68)	4.1	1.682	.002	.064	.007	1.008	.005	2.556	.151	1.226	.012	20	24	35	32	.983, .026
27-10	101	4.1	1.872	.102	.042	.007	1.558	.135	2.241	.266	1.338	.042	2	3	5	7	.988, .033
28-10	138	4.1	1.966	.112	.041	.008	1.273	.095	2.315	.224	1.330	.031	4	5	9	6	.889, .214
29-10	210	4.1	2.056	.091	.042	.007	1.180	.075	2.480	.228	1.354	.035	4	6	7	5	.785, .371
30-10	247	4.1	2.078	.099	.042	.007	1.109	.055	2.534	.196	1.373	.028	4	5	7	11	.989, .025
31-10	286	4.1	2.067	.068	.041	.007	1.079	.040	2.730	.221	1.383	.035	5	6	9	2	.238, .908
01-11	303	4.1	2.089	.079	.045	.008	1.110	.053	2.684	.194	1.381	.034	4	5	6	4	.628, .566

In addition, the forecasting model is applied to the other sequences in Table 1 (A to E), starting about 1 to 2 hours following their mainshocks. The forecasting results for the first 24 hours are shown in Figure 6 for sequences A to E. As seen in Figure 6, it is confirmed that the numbers of forecasted events are in good agreement with the observed data. Additionally, in all the six considered sequences the forecasted events' spatial distribution is also in good agreement with the observed data. This is evidence that the proposed model can reproduce seismic sequences surrounding a mainshock in the study area.

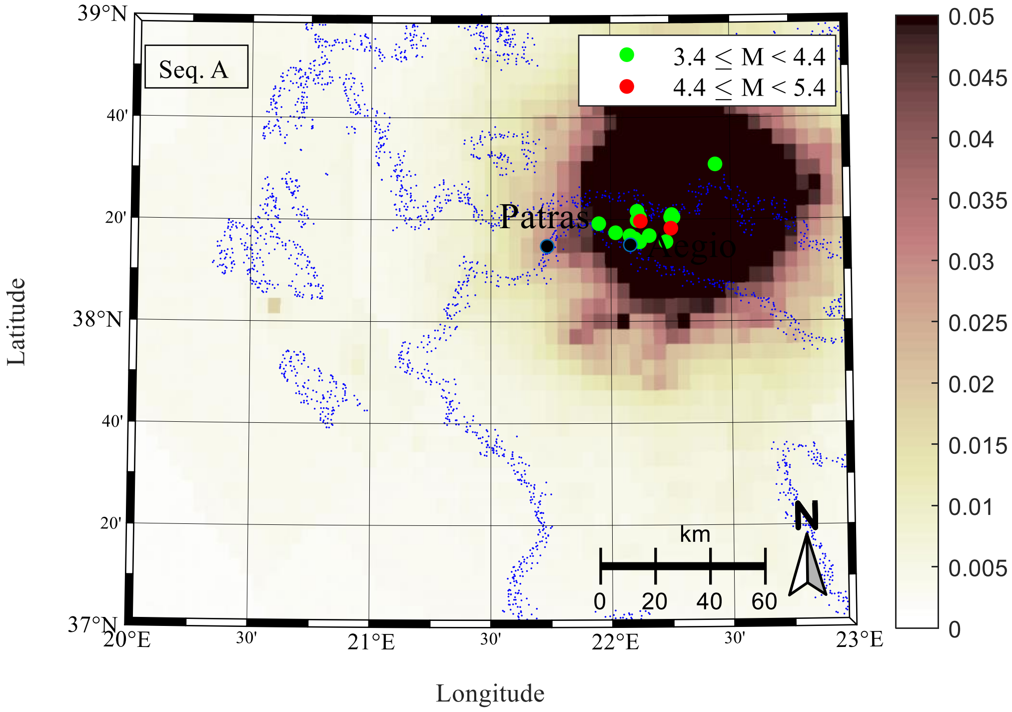

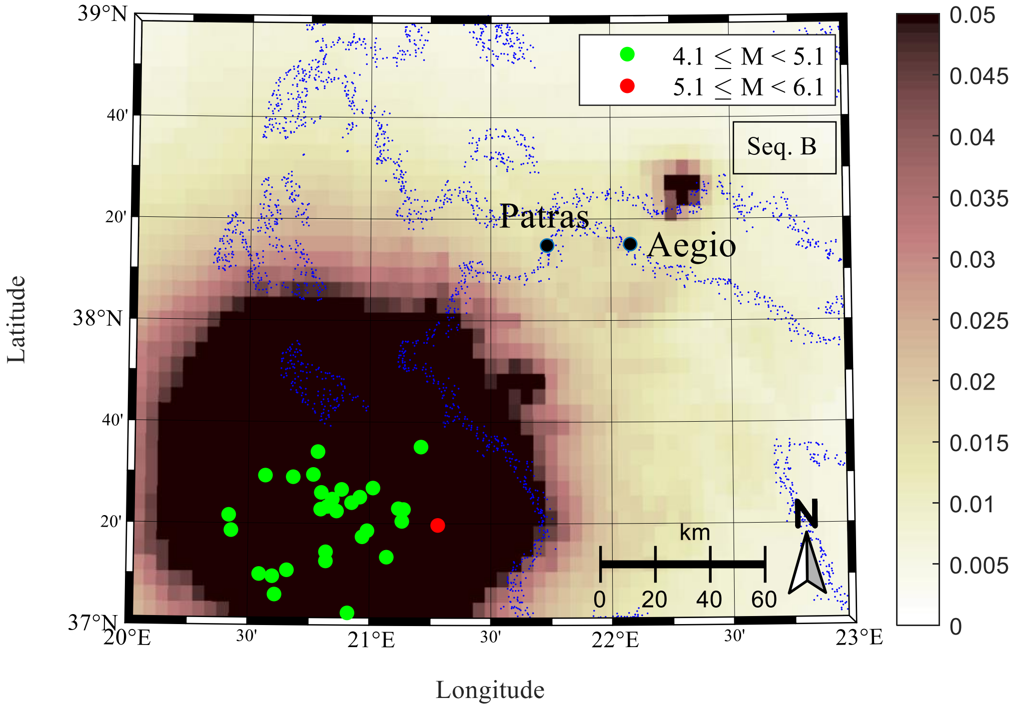
39°N
40'
20'
38°N
40'
20'
37°N
20°E
30'
21°E
30'
22°E
30'
23°E
Latitude
Longitude
4.1 ≤ M < 5.1
5.1 ≤ M < 6.1
Seq. B
Patras
Aegio
km
0 20 40 60
N
0.05
0.045
0.04
0.035
0.03
0.025
0.02
0.015
0.01
0.005
0

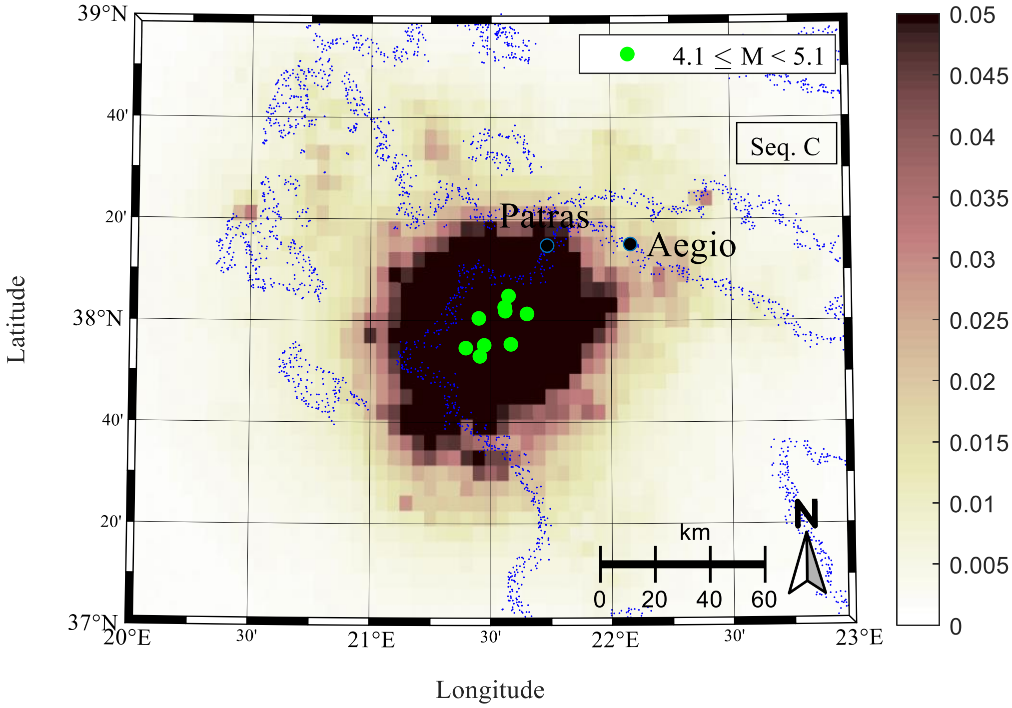

39°N
40'
20'
38°N
40'
20'
37°N
20°E
30'
21°E
30'
22°E
30'
23°E
Latitude
Longitude
4.1 ≤ M < 5.1
Seq. C
Patras
Aegio
km
0
20
40
60
N
0.05
0.045
0.04
0.035
0.03
0.025
0.02
0.015
0.01
0.005
0

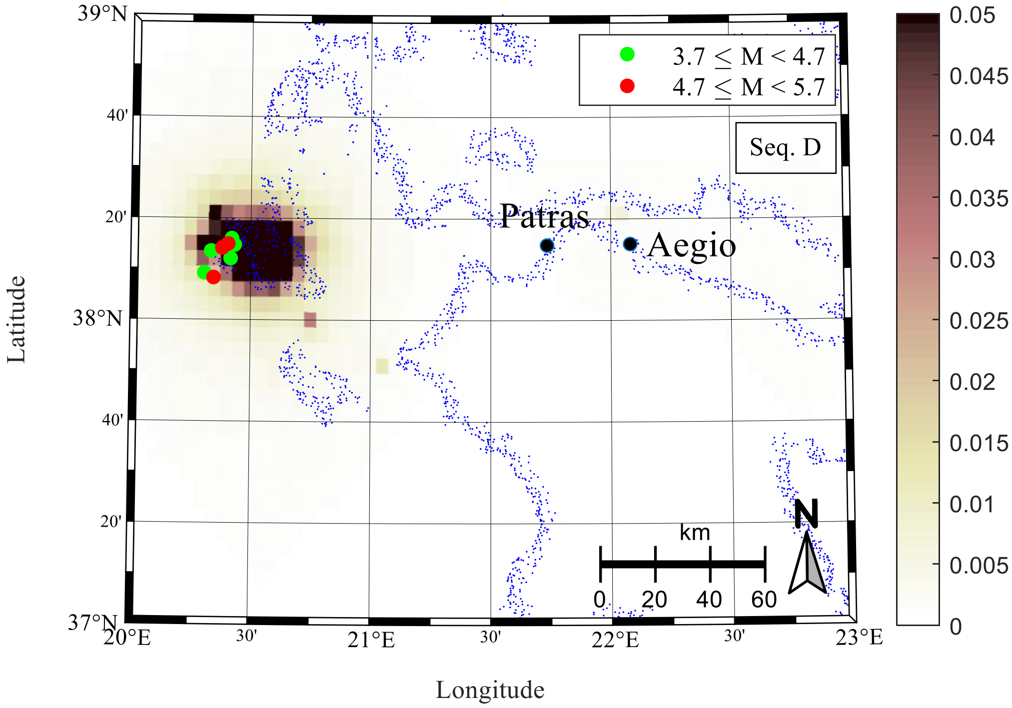

39°N
40'
20'
38°N
40'
20'
37°N
20°E
30'
21°E
30'
22°E
30'
23°E
Latitude
Longitude
3.7 ≤ M < 4.7
4.7 ≤ M < 5.7
Seq. D
Patras
Aegio
km
0
20
40
60
N
0.05
0.045
0.04
0.035
0.03
0.025
0.02
0.015
0.01
0.005
0

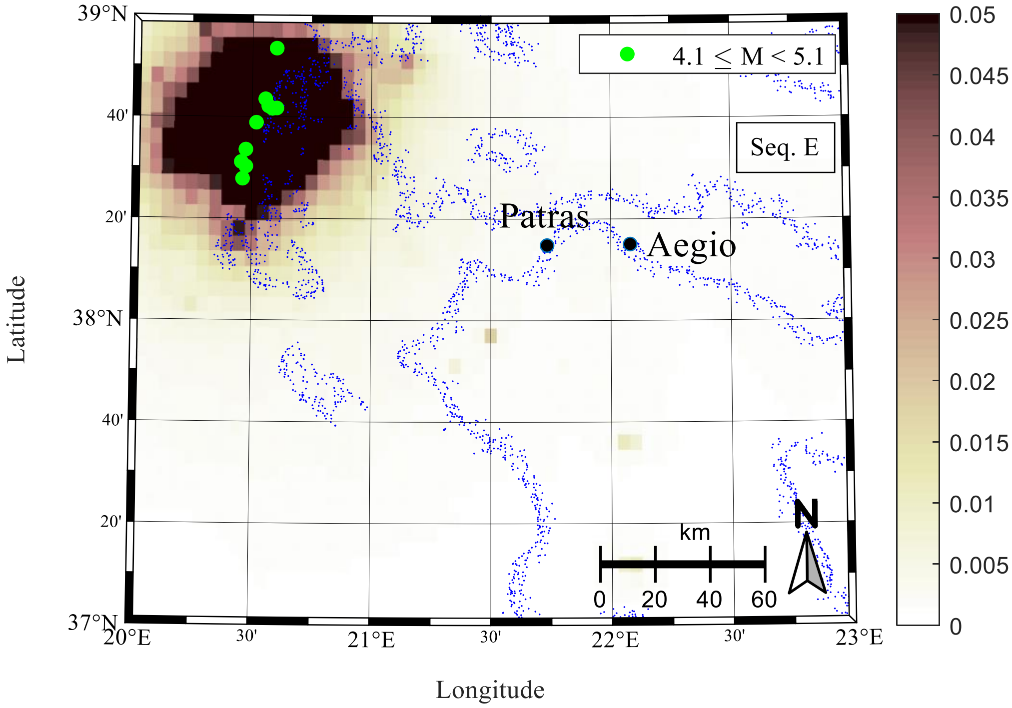

Figure 6. The spatial distribution of seismicity (the maps report the mean+2 **σ** confidence interval, i.e. 98th percentile, for the number of events per km^2) in the aftershock zone for sequences A to E (Table 1) during one day following the mainshock. See the caption of Figure 5 for an explanation of the information.

As discussed earlier, one concern in the ETAS forecasting approach is how to select reasonable prior values for **θ**. The posterior distributions of **θ**, in the day following the mainshock, and for the six seismic sequences in Table 1, are shown in Table 6. The forecasting origin time, T_{start}, for each seismic sequence in Table 6 is identical to that shown in Figures 5 and 6. The median of the five model parameters of ETAS and their uncertainties are also provided in Table 6. Furthermore, the minimum and maximum values for each model parameter (in terms of the median and **σ**) are shown in the last row in Table 6, which we propose to be employed as a reasonable set of prior **θ** for further implementation in the study area. As seen in Table 6, parameters c and p do not change significantly, confirming that the temporal decay follows the MO's law in all the sequences. However, parameters β

and *d* vary significantly among the different sequences, which indicates that the spatial characteristics and the Gutenberg-Richter relation are sequence-specific. Additionally, it is worth emphasising that, as seen in Table 6, the ETAS posterior parameters are quite sequence-specific. Hence, using the proposed *incremental adaptive training algorithm* is a superior approach to using the model parameters from previous sequences in the study area.

Table 6. The posterior distributions of ETAS parameters for six sequences in Table 1. All the parameters are assumed normally distributed.

Sequence ID	β		c		p		d		q	
	median	σ	median	σ	median	σ	median	σ	median	σ
A	2.049	.001	.062	.008	1.010	.004	2.669	.221	1.195	.010
B	2.148	.016	.042	.008	1.018	.009	2.153	.216	1.187	.018
C	2.270	.012	.055	.007	1.010	.006	2.457	.212	1.217	.015
D	2.151	.091	.031	.008	1.033	.024	1.172	.199	1.182	.032
E	1.759	.069	.046	.007	1.012	.007	1.654	.193	1.216	.023
F	1.682	.002	.064	.007	1.008	.005	2.556	.151	1.226	.012
Bounds of parameters	1.682-2.270	.001-.091	.031-.064	.007-.008	1.008-1.033	.004-.024	1.172-2.669	.151-.221	1.182-1.226	.010-.032

6 SEISMIC HAZARD MODEL

The short-term changes in seismicity revealed by the ETAS model, reflected by the time-variant conditional rate in Equation 1, are superimposed on the background seismicity (see Equation 2) to forecast the number of events over the aftershock zone within the considered time interval. The seismicity output in terms of the forecasted number of events in the forecasting time interval can be used as the short-term seismicity rate within a short-term time-dependent PSHA. Therefore, firstly, a conventional PSHA has been performed using Equation 6 (adapted from Cornell 1968; McGuire 1995; Ebrahimian et al 2014; Baker 2015; Ebrahimian et al. 2019; and numerically integrated over the aftershock zone):

$$\lambda(PGA > pga) = \lambda(M > M_{min}) \int_{M_{min}}^{M_{max}} \int_{X_{min}}^{X_{max}} \int_{Y_{min}}^{Y_{max}} P(PGA > pga|m, d\{(x,y),(x_s,y_s)\}).\, f_M(m).\, f_{X,Y}(x,y)\, \mathrm{d}y\mathrm{d}x\mathrm{d}m \quad \text{(Eq. 6)}$$

where $\lambda(PGA > pga)$ is the annual rate of exceedance of *PGA* above a threshold *pga*; M_{min} is equal to 4.5 (the same assumption as in ESHM13); M_{max} is the maximum magnitude obtained from the ESHM13 results for each area source; $\lambda(M > M_{min})$ is the annual rate of exceedance of earthquakes greater than M_{min}, which is numerically defined for each grid cell based on the ESHM13 SEIFA model; $d\{(x,y),(x_s,y_s)\}$ is the epicentral distance between the desired site (x_s and y_s coordinates where the hazard computation is of interest) and an arbitrary point (x and y coordinates ∈ **A**) inside the aftershock zone (see also Ebrahimian et al. 2019); $P(PGA > pga|m, d\{(x,y),(x_s,y_s)\})$ is the conditional probability of *PGA* exceeding a threshold *pga*, given a magnitude *m* and an epicentral distance *d* at the (x,y ∈ **A**) coordinate which can be estimated using a Ground Motion Prediction Equation (GMPE); $f_M(m)$ is the probability density function of magnitude, which follows the Gutenberg-Richter relationship based on the ESHM13 for each area source; $f_{X,Y}(x,y)$ is the joint probability density function of the distance distribution at an arbitrary point with (x,y ∈ **A**) from the site (x_s,y_s) coordinate, which has a uniform distribution, i.e. assuming equiprobable occurrence of earthquakes in the area source; X_{min} and X_{max} are, respectively, the lower and upper bound values in the x-axis direction in Cartesian coordinates inside the study area (∈ **A**); Y_{min} and Y_{max} are, respectively, the lower and upper bound values in the y-axis direction in Cartesian coordinates inside the study area (∈ **A**).

Choosing GMPEs for seismic hazard analysis has always been a challenging task (see also Danciu et al. 2007; Segou et al. 2010; Delavaud et al. 2012; Skarlatoudis et al. 2013). On the other hand, a sophisticated logic tree including several GMPEs makes the forecasting algorithm time consuming, thereby limiting its potential real-time use for OEF. Therefore, only three GMPEs are used in this study to approximately match the ESHM13 assumptions as well as recent GMPE developments for Greece: Chiou and Youngs (2014), with a weight of 25%, Zhao et al. (2006), with a weight of 25%, and Boore et al. (2021), with a weight of 50%. The 2008 version of Chiou and Youngs' GMPE has been used in ESHM13; however, we decided to use the newer version (Chiou and Youngs 2014). The Chiou and Youngs (2014) GMPE is also justified by this model's high stability (Bommer and Stafford 2020). However, Zhao et al. (2006) GMPE was also chosen to account for epistemic uncertainty since it has the simplest functional form among the GMPEs used in the ESHM13. The Boore et al. (2021) GMPE was also taken into consideration since it has recently been developed specifically for Greece. Therefore, we allocate a higher, 50%, weight to this regional model. We also acknowledge that the influence of GMPE selection on the final short-term time-dependent PSHA is an interesting topic for future research but it is beyond the scope of this study.

The short-term (daily) time-dependent PSHA is performed by substituting the rate $\lambda(M > M_{min})$ in Equation (6) by the forecasted number of events obtained from the robust seismicity framework (herein, corresponding to sequence F for 26 October 2018) and over the forecasting time interval (see Equation 4). The rest of the parameters have the same definition and values as used for the background (time-independent) hazard calculations. The aftershock zone is subdivided into 14 area sources as defined in ESHM13 and shown in Figure 7. The results of the conventional and time-dependent PSHA are shown in Figure 8 for Patras city. The left graph in Figure 8 is for the daily probability of exceedance, and the right graph is for the daily rate of exceedance. It is assumed that a Poisson process models the occurrence of earthquakes of interest. It is worth mentioning that a complex logic-tree is not recommended for OEF, since the computational effort should be kept to a minimum level to obtain the forecasts as rapidly as possible.

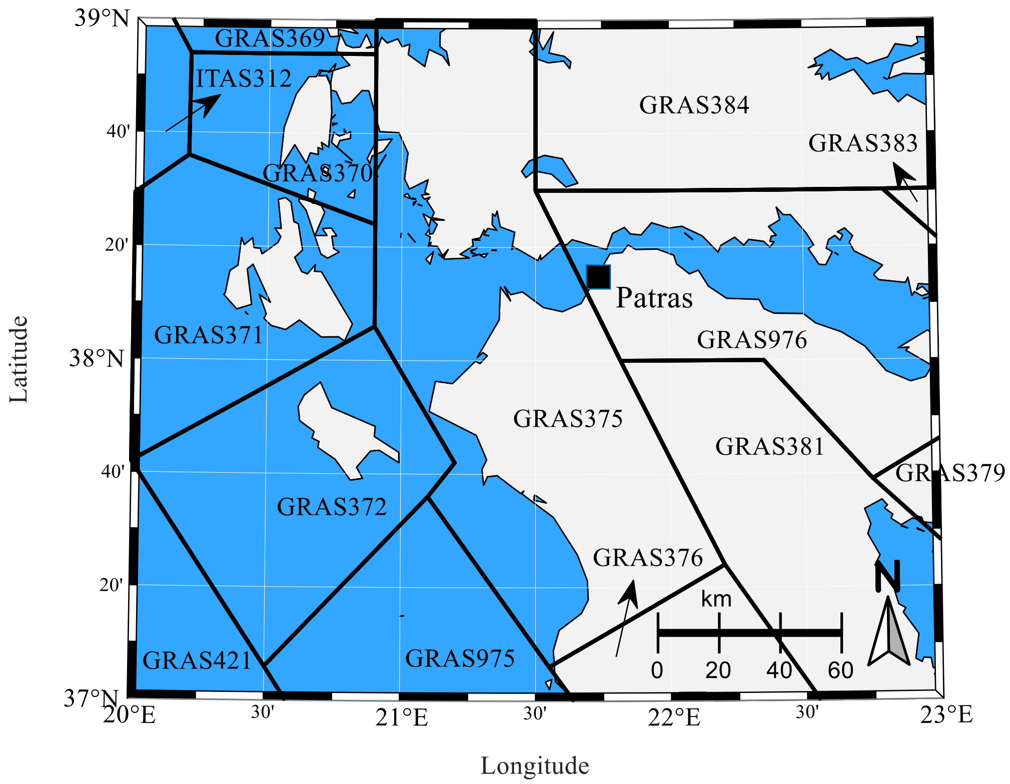

Figure 7. 14 area sources in the study area from ESHM13 (Giardini et al. 2013; Woessner et al. 2015).

In the next step, $\lambda(M > M_{min})$ is altered with the expected number of events within the forecasting interval (herein, 1-day) resulting from the implemented seismicity forecasting framework to account for the summation of background seismicity (from conventional PSHA) and short-term seismicity (see Equation 4). The hazard integral (Equation 5) is computed again based on this increased short-term seismicity. The results of this time-dependent PSHA are shown in the left (daily probability of exceedance) and the right (daily rate of exceedance) panels in Figure 8 for Patras on 26 October 2018. For the purpose of comparison with the conventional PSHA, the annual frequency of exceedance derived from the long-term (time-independent) hazard is converted to the daily rate (dividing by 365) and consequently transformed into the daily probability of exceedance using the Poisson distribution. It is worth mentioning that the conventional hazard curve represents a lower bound for this short-term hazard curve, since we assume that the short-term seismicity can only increase the long-term hazard.

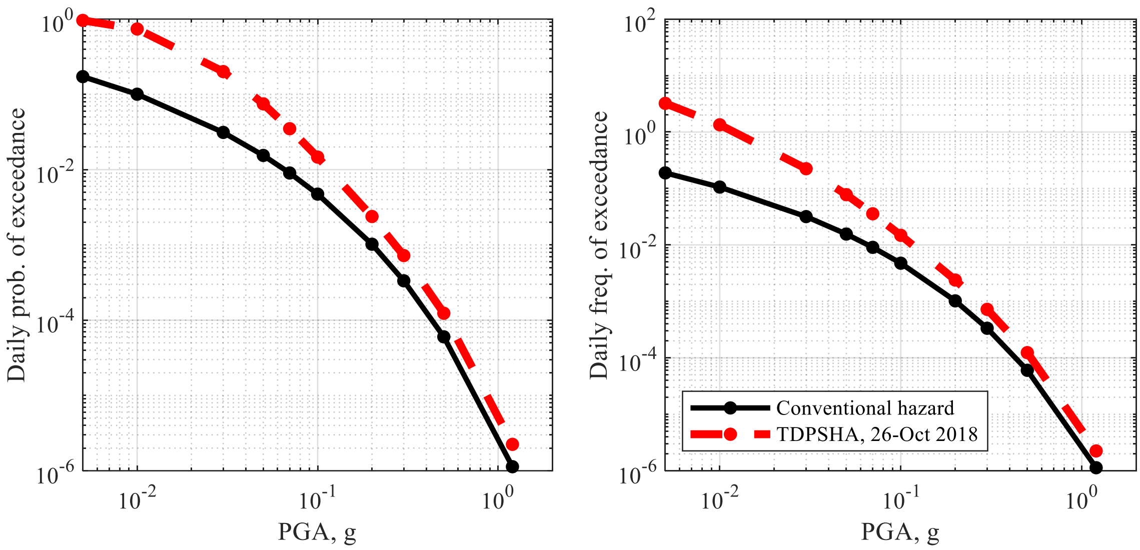

Figure 8. Short-term PSHA for Patras, (left): the short-term time-dependent daily probability of exceedance versus *PGA* and comparison with the conventional daily hazard curve, and (right): short-term time-dependent daily rate of exceedance versus *PGA* and comparison with the conventional daily hazard curve.

The short-term hazard ratio to the median conventional hazard is defined as the *Probability Gain* (PG), which is a function of the considered *PGA*. As can be seen in Figure 8, the PG parameter decreases as PGA increases. The PG parameter, corresponding to a *PGA* equal to 0.05g, is calculated for all the cells inside the study area and the results are shown in Figure 9 in terms of 2nd, 50th, and

98th percentiles. These percentiles are based on the dispersion of the forecasted number of events obtained from the robust seismicity framework. It is worth mentioning that the background seismicity is kept to the median value for all three cases. The maximum PG values occur around the mainshock's epicentre, and equal 321, 385, and 448, respectively, in the cases of 2nd (Figure 9-top), 50th (Figure 9-middle), and 98th percentiles (Figure 9-bottom). However, the colour bar in Figure 9 is limited to 100 to better distinguish the differences amongst the cells.

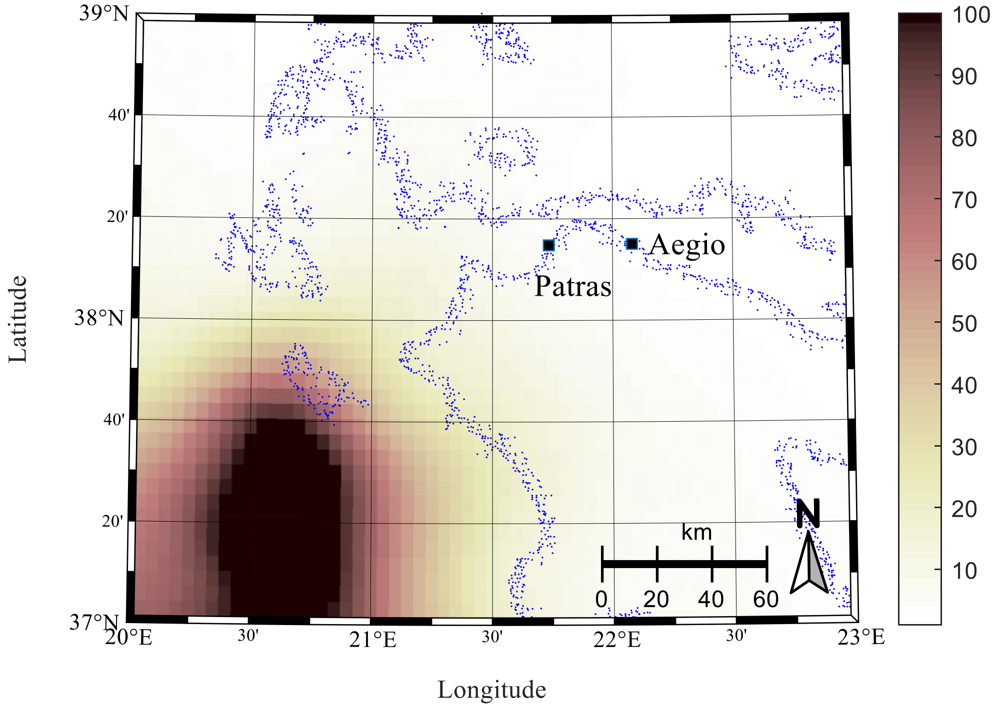

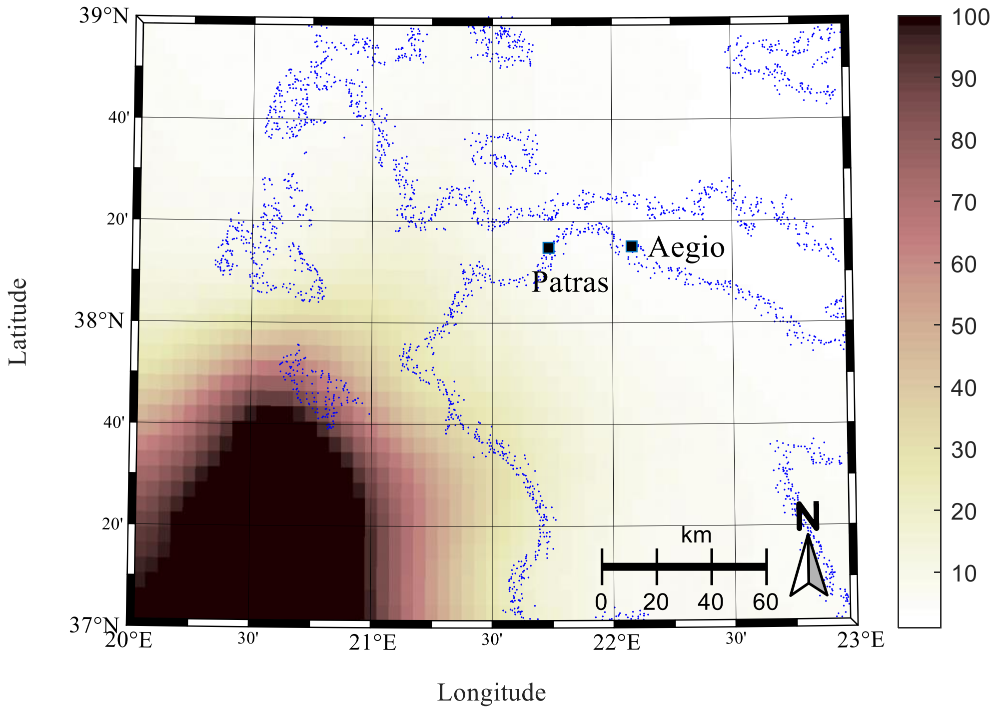

39°N
40'
20'
38°N
40'
20'
37°N
20°E
30'
21°E
30'
22°E
30'
23°E
Latitude
Longitude
Patras
Aegio
km
0
20
40
60
N
100
90
80
70
60
50
40
30
20
10

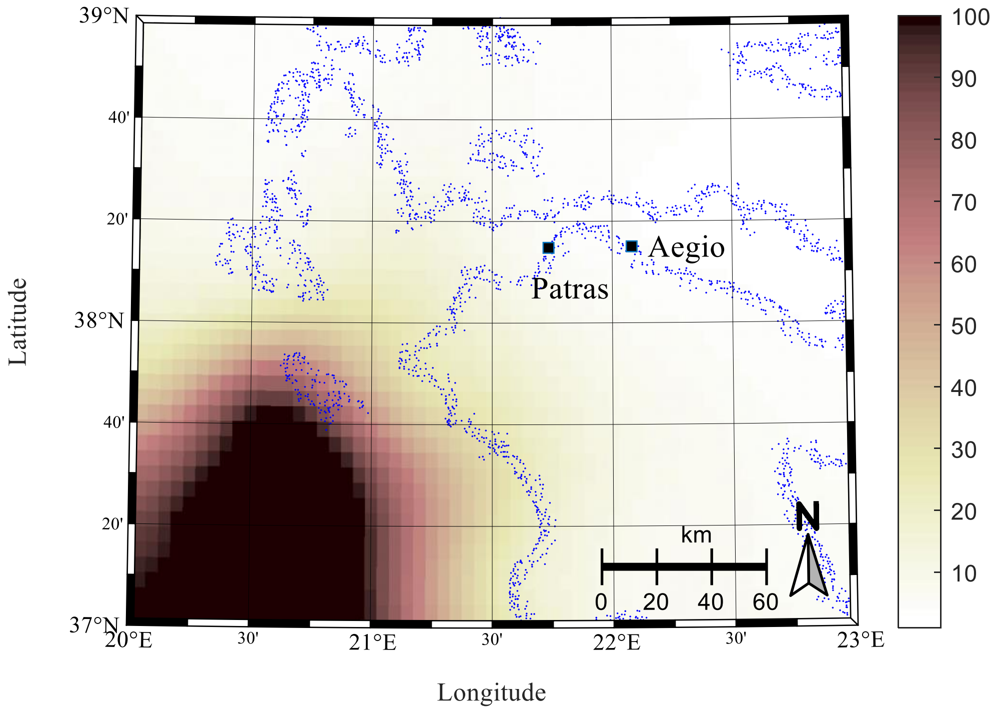

Figure 9. The spatial distribution of the PG parameter (the ratio of short-term hazard to the long-term time-independent hazard corresponding to a *PGA* equal to 0.05g) for sequence F (Table 1). The forecast starts at 00:00UTC on 26 October 2018 and for the next 24 hours. (top): 2nd percentile, (middle): 50th percentile, and (bottom): 98th percentile.

PG can also be considered for a given site with respect to time since the mainshock. The variation of the 50th percentile PG for the cities of Patras and Aegio is shown in Figure 10 for all the sequences in Table 1 during the four days following each sequence's mainshock. The results reveal that the heightened seismicity decays rapidly during the first two days (the so-called "golden hours" for first responders) following the mainshock. The 50th percentile PG is as high as 33 in Aegio (23 km from the epicentre of the mainshock of sequence A, see Table 1) during the first hours following the mainshock whereas, the 50th percentile PG equals 17 in Patras (50 km from the epicentre) in this time period. As seen in Figure 10, the same trend is seen for sequence C (see Table 1), the second closest event to the studied cities among the six selected sequences. The other seismic sequences show lower

PG values (mostly less than 10) since their mainshock epicentres are far from the studied cities. For example, the 50th percentile PG value is about 3 in the case of sequence F (starting on 26 October 2018), which can also be seen in Figure 8 for a *PGA* equal to 0.05g.

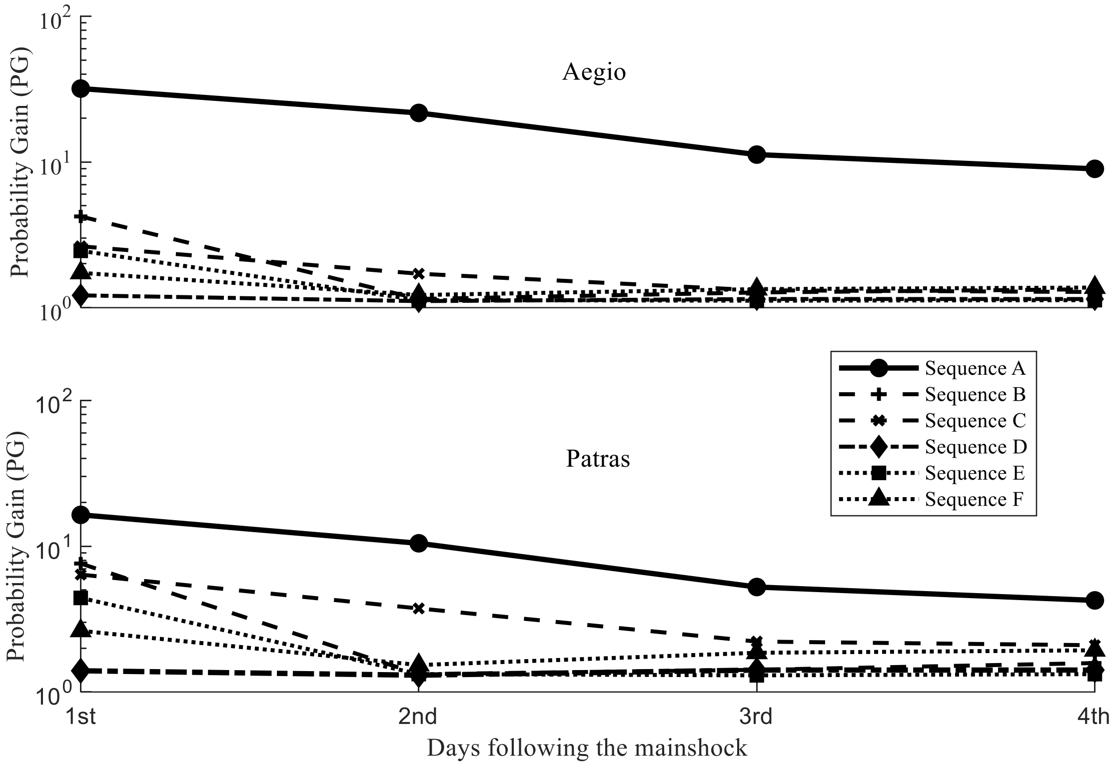

Figure 10. The median probability gain PG (the ratio of the median short-term time-dependent to the median long-term time-independent hazard corresponding to a *PGA* equal to 0.05g) versus days since the mainshock at Patras and Aegio for the different seismic sequences in Table 1.

7 CONCLUSIONS

A robust seismicity forecasting framework has been applied using the ISC earthquake catalogue for western Greece, one of the most seismically active regions in Europe. The chosen catalogue was used to identify six aftershock sequences between 1995 to 2018 with at least one mainshock with moment magnitude Mw ≥ 6. A new approach has been introduced for incrementally adaptive training of the ETAS model parameters prior to the mainshock, which can be further used to start forecasting quickly after the mainshock. The developed algorithm facilitates the concept of operational earthquake forecasting, which aims at forecasting damaging earthquakes during the first golden hours after a severe mainshock. It is worth emphasising that the employed algorithm takes advantage of Bayesian inference, in contrast to the majority of the available studies which use constant ETAS coefficients. The forecasting algorithm is applied for the next 24 hours to forecast the spatial distribution of the seismicity rate and the number of potentially damaging earthquakes (here defined as an event with a moment magnitude Mw ≥ 4.5). In addition, the proposed algorithm has been tested to demonstrate its usability for operational forecasting on the basis of intervals of 6 hours to 7 days. The results show that the adapted ETAS model within the seismicity framework can retrospectively forecast the number of damaging earthquakes and that the forecasts are generally in good agreement with the observed data. The spatial distribution of the heightened seismicity zone is also in good agreement with the spatial propagation of observed events. This seismicity forecasting framework has been applied to the six selected seismic sequences, and posterior distributions of the model parameters were obtained by employing Bayesian inference. These distributions and their relative bounds are proposed as prior values for future forecasting of new aftershock sequences in the region. The results of the current study reveal that the temporal decay of events follows almost the same MO's law for all sequences; however, the spatial and magnitude-frequency (Gutenberg-Richter) characteristics are sequence-specific.

The forecasted occurrence rates were implemented within a time-dependent seismic hazard framework using inputs on the long-term seismicity from ESHM13. The daily seismic hazard was computed for the study area as well as for the two major cities of the study region, Patras and Aegio. The results revealed that the daily probability of exceeding a threshold *PGA* equal to 0.05g is, on average, increased by up to 33 times the long-term (time-independent) hazard in Aegio, during the first hours following the 1995 Mw 6.5 mainshock. This PG parameter decays to under 10 after three days. Additionally, the PG parameter varies between 1 and 10 for the four seismic sequences (B, D, E and F) that are relatively far from the considered cities. It is important to note that multiple types of uncertainty have been addressed in the proposed forecasting framework, such as Bayesian inference and MCMC simulations in the ETAS forecasting model, and GMPE and logic-tree in the hazard model. However, the optimum choice of GMPE and associated logic-tree weights for this region, and more generally for operational earthquake forecasting globally, remains an interesting topic for future research. Also, considering uncertainties from different sources such as the PSHA and forecasting algorithms is an area to be explored in future.

The current study has demonstrated the applicability of the proposed forecasting algorithm for short-time intervals (by emphasising medium-to-large events), which is of great interest for first responders during an aftershock sequence. The forecasted distribution was in good agreement with the observed events in all retrospectively-studied earthquake sequences. Besides, the spatial distribution of forecasted events was close to the distribution of observed events. Therefore, at least within the assumption and limitations of the present study, it is concluded that the employed Bayesian inference has the ability to be adapted to the specific characteristics of earthquakes in this region.

Acknowledgements

This study was supported by the European Union's Horizon 2020 research and innovation programme under grant agreement No 821046, project TURNkey (Towards more Earthquake-resilient Urban Societies through a Multi-sensor-based Information System enabling Earthquake Forecasting, Early Warning and Rapid Response actions). We thank the partners of Workpackage 3 of TURNkey and the project management team for their comments on these analyses. Finally, we thank two anonymous reviewers and the journal editor (Dr Margarita Segou) for their detailed and constructive comments on earlier versions of this manuscript in which substantially enhanced the paper's quality.

DATA AVAILABILITY

Earthquake catalogue data were provided by ISC (last accessed 2020). The data regarding this article can be found online at https://earthquake-turnkey.eu/ or by contacting the corresponding author.

REFERENCES

Azarbakht, A., Rudman, A., & Douglas, J. (2021). A decision-making approach for operational earthquake forecasting. *International Journal of Disaster Risk Reduction*, **66**, p1-13.

Baker, J. W. (2015) Introduction to Probabilistic Seismic Hazard Analysis. White Paper Version 2.1, 77 pp.

Beck, J. L. & Au, S. K. (2002) Bayesian updating of structural models and reliability using Markov Chain Monte Carlo simulation. *Journal of Engineering Mechanics ASCE*, **128(**4), 380-391.

Bommer, J. J., & Stafford, P. J. (2020). Selecting Ground-Motion Models for Site-Specific PSHA: Adaptability versus Applicability. *Bulletin of the Seismological Society of America*, **110**(6), 2801-2815.

Bondár, I., & Storchak, D. (2011). Improved location procedures at the International Seismological Centre. *Geophysical Journal International*, **186**(3), 1220-1244.

Boore, D. M., Stewart, J. P., Skarlatoudis, A. A., Seyhan, E., Margaris, B., Theodoulidis, N., Scordilis, E., Kalogeras, I., Klimis, N. and Melis, N. S. (2021). A ground-motion prediction model for shallow crustal earthquakes in Greece. *Bulletin of the Seismological Society of America*, **111**(2), 857-874. Cattania, C., Werner, M. J., Marzocchi, W., Hainzl, S., Rhoades, D., Gerstenberger, M., ... & Jordan, T. H. (2018). The forecasting skill of physics-based seismicity models during the 2010‐2012 Canterbury, New Zealand, earthquake sequence. *Seismological Research Letters*, 89(4), 1238-1250.

Chiou, B. S. J., & Youngs, R. R. (2014). Update of the Chiou and Youngs NGA model for the average horizontal component of peak ground motion and response spectra. *Earthquake Spectra*, **30**(3), 1117-1153.

Console, R., Rhoades, D. A., Murru, M., Evison, F. F., Papadimitriou, E. E., & Karakostas, V. G. (2006). Comparative performance of time-invariant, long-range and short-range forecasting models on the earthquake catalogue of Greece. *Journal of Geophysical Research: Solid Earth*, **111**(B9).

Console, R., Murru, M., Catalli, F., Falcone, G. (2007). Real time forecasts through an earthquake clustering model constrained by the rate-and-state constitutive law: comparison with a purely stochastic ETAS model. *Seismological Research Letters*, **78**(1), 49–56.

Cornell, C. A. (1968). Engineering seismic risk analysis. *Bulletin of the seismological society of America*, **58**(5), 1583-1606.

Daley, D. J., & Vere-Jones, D. (2008). An introduction to the theory of point processes: volume II: general theory and structure. *Springer New York*.

Danciu, L., & Tselentis, G. A. (2007). Engineering ground-motion parameters attenuation relationships for Greece. *Bulletin of the Seismological Society of America*, **97**(1B), 162-183.

Delavaud, E., Cotton, F., Akkar, S., Scherbaum, F., Danciu, L., Beauval, C., Drouet, S., Douglas, J., Basili, R., Sandikkaya, M.A. and Segou, M. (2012). Toward a ground-motion logic tree for probabilistic seismic hazard assessment in Europe. *Journal of Seismology*, **16**(3), 451-473.

Douglas, J., & Azarbakht, A. (2021). Cost–benefit analyses to assess the potential of Operational Earthquake Forecasting prior to a mainshock in Europe. *Natural Hazards*, **105**(1), 293-311.

Drakatos, G., & Latoussakis, J. (1996). Some features of aftershock patterns in Greece. *Geophysical Journal International*, **126**(1), 123-134.

Ebrahimian H., Jalayer F. (2021). Operational Aftershock Forecasting for 2017-2018 Seismic Sequence in Western Iran. *EGU General Assembly*, Online, 19-30 April 2021, EGU21-15824, https://doi.org/10.5194/egusphere-egu21-15824.

Ebrahimian, H., Jalayer, F., Forte, G., Convertito, V., Licata, V., d'Onofrio, A., ... & Manfredi, G. (2019). Site-specific probabilistic seismic hazard analysis for the western area of Naples, Italy. *Bulletin of earthquake engineering*, *17*(9), 4743-4796.

Ebrahimian, H., & Jalayer, F. (2017). Robust seismicity forecasting based on Bayesian parameter estimation for epidemiological spatio-temporal aftershock clustering models. *Scientific reports*, **7**(1), 1-15.

Ebrahimian, H., Jalayer, F., Asprone, D., Lombardi, A. M., Marzocchi, W., Prota, A., & Manfredi, G. (2014). Adaptive daily forecasting of seismic aftershock hazard. *Bulletin of the Seismological Society of America*, **104**(1), 145-161.

Ebrahimian H., Jalayer F., Asprone D., Lombardi A.M., Marzocchi W., Prota A., Manfredi G. (2014). A performance-based framework for adaptive seismic aftershock vulnerability assessment. *Earthquake Engineering and Structural Dynamics*, 43(14): 2179-2197.

Ebrahimian H., Jalayer F., Asprone D., Lombardi A.M., Marzocchi W., Prota A., and Manfredi G. (2013). An outlook into time-dependent aftershock vulnerability assessment. *4^{th} ECCOMAS Thematic Conference on Computational Methods in Structural Dynamics and Earthquake Engineering (COMPDYN2013)*, M. Papadrakakis, V. Papadopoulos, V. Plevris (eds.), Kos Island, Greece, 12-14 June 2013.

Field, E. H., & Milner, K. R. (2018). Candidate products for operational earthquake forecasting illustrated using the HayWired planning scenario, including one very quick (and not-so-dirty) hazard-map option. *Seismological Research Letters*, *89*(4), 1420-1434.

Giardini, D, J Woessner, L Danciu, H Crowley, F Cotton, G Grünthal, R Pinho, et al., 2013. Seismic Hazard Harmonisation in Europe (SHARE): Online Data Resource. doi: 10.12686/SED-00000001-*SHARE*.

Goltz, J. D., 2015. A Further Note on Operational Earthquake Forecasting: An Emergency Management Perspective. *Bulletin of the Seismological Society of America*, **86**(5) 1231-1233.

Gospodinov, D., Karakostas, V., Papadimitriou, E., & Ranguelov, B. (2007). Analysis of relaxation temporal patterns in Greece through the RETAS model approach. *Physics of the Earth and Planetary Interiors*, **165**(3-4), 158-175.

Gospodinov, D., & Rotondi, R. RETAS: a restricted ETAS model inspired by Bath’s law. The 4th International Workshop on Statistical Seismology – The Graduate University for Advanced Studies, Shonan Village campus, Kanagawa Prefecture, Japan, 9-13 January, 2006.

Hainzl, S., Christophersen, A., & Enescu, B. (2008). Impact of earthquake rupture extensions on parameter estimations of point-process models. *Bulletin of the Seismological Society of America*, 98(4), 2066-2072.

Hainzl, S., Zakharova, O., & Marsan, D. (2013). Impact of aseismic transients on the estimation of aftershock productivity parameters. *Bulletin of the Seismological Society of America*, 103(3), 1723-1732.

Harte, D. S. (2013). Bias in fitting the ETAS model: a case study based on New Zealand seismicity. *Geophysical Journal International*, 192(1), 390-412.

Hastings, W. K. (1970). Monte-Carlo sampling methods using Markov chains and their applications. *Biometrika*, 57(1), 97-109.

International Seismological Centre (2020), On-line Bulletin, https://doi.org/10.31905/D808B830

Jordan, T. H., Marzocchi, W., Michael, A. J., & Gerstenberger, M. C. 2014. Operational Earthquake Forecasting Can Enhance Earthquake Preparedness. *Seismological Research Letters*, **85**(5): 955–59.

Jordan, T. H., & Jones, L. M. (2010). Operational earthquake forecasting: Some thoughts on why and how. *Seismological Research Letters*, **81**(4), 571-574.

Karagianni, E., Paradisopoulou, P., & Karakostas, V. (2013). Spatio-temporal earthquake clustering in the Western Corinth Gulf. *Bulletin of the Geological Society of Greece*, **47**(3), 1109-1117.

Karakostas, V., Kostoglou, A., Chorozoglou, D., & Papadimitriou, E. (2020). Relocation of the 2018 Zakynthos, Greece, aftershock sequence: spatiotemporal analysis deciphering mechanism diversity and aftershock statistics. *Acta Geophysica*, **68**(5), 1263-1294.

Karakostas, V., Papadimitriou, E., & Gospodinov, D. (2014). Modelling the 2013 North Aegean (Greece) seismic sequence: geometrical and frictional constraints, and aftershock probabilities. *Geophysical Journal International*, **197**(1), 525-541.

Kourouklas, C., Mangira, O., Iliopoulos, A., Chorozoglou, D., & Papadimitriou, E. (2020). A study of short-term spatiotemporal clustering features of Greek seismicity. *Journal of Seismology*, **24**, 459-477.

Latoussakis, J., & Drakatos, G. (1994). A quantitative study of some aftershock sequences in Greece. *pure and applied geophysics*, **143**(4), 603-616.

Latoussakis, J., Stavrakakis, G., Drakopoulos, J., Papanastassiou, D., & Drakatos, G. (1991). Temporal characteristics of some earthquake sequences in Greece. *Tectonophysics*, **193**(4), 299-310.

Lippiello, E., Petrillo, G., Godano, C., Tramelli, A., Papadimitriou, E., & Karakostas, V. (2019). Forecasting of the first hour aftershocks by means of the perceived magnitude. *Nature communications*, **10**(1), 1-10.

Lippiello, E., Cirillo, A., Godano, G., Papadimitriou, E., & Karakostas, V. (2016). Real-time forecast of aftershocks from a single seismic station signal. *Geophysical Research Letters*, **43**(12), 6252-6258.

Lippiello, E., Giacco, F., Arcangelis, L. D., Marzocchi, W., & Godano, C. (2014). Parameter estimation in the ETAS model: Approximations and novel methods. *Bulletin of the Seismological Society of America*, **104**(2), 985-994.

Lippiello, E., Marzocchi, W., De Arcangelis, L., & Godano, C. (2012). Spatial organisation of foreshocks as a tool to forecast large earthquakes. *Scientific reports*, *2*(1), 1-6.

Marzocchi, W., & Lombardi, A. M. (2009). Real-time forecasting following a damaging earthquake. *Geophysical Research Letters*, 36(21).

Marzocchi, W., and M. Murru (2012), Daily earthquake forecasts during the May–June 2012 Emilia earthquake sequence (northern Italy), *Annals of Geophysics*, 55(4), 561–567, doi:10.4401/ag-6161.

Marzocchi, W., Lombardi, A. M., & Casarotti, E. (2014). The establishment of an operational earthquake forecasting system in Italy. *Seismological Research Letters* 85(5): 961-969.

Mangira, O., Console, R., Papadimitriou, E., Murru, M., & Karakostas, V. (2020). The short-term seismicity of the Central Ionian Islands (Greece) studied by means of a clustering model. *Geophysical Journal International*, *220*(2), 856-875.

McBride, S. K., Llenos, A. L., Page, M. T., & Van Der Elst, N. (2020). # EarthquakeAdvisory: Exploring discourse between government officials, news media, and social media during the 2016 Bombay Beach Swarm. *Seismological Research Letters*, **91**(1), 438-451.

McGuire, R. K. (1995). Probabilistic seismic hazard analysis and design earthquakes: closing the loop. *Bulletin of the Seismological Society of America*, **85**(5), 1275-1284.

Metropolis, N., Rosenbluth, A. W., Rosenbluth, M. N., Teller, A. H., Teller, E. (1953). Equations of state calculations by fast computing machines. *Journal of Chemical Physics* **21**(6), 1087-1092.

Ogata, Y., & Zhuang, J. (2006). Space–time ETAS models and an improved extension. *Tectonophysics*, **413**(1-2), 13-23.

Ogata, Y. (1998). Space-time point-process models for earthquake occurrences. *Annals of the Institute of Statistical Mathematics*, **50**(2), 379-402.

Ogata, Y. (1988). Statistical models for earthquake occurrences and residual analysis for point processes. *Journal of the American Statistical association*, **83**(401), 9-27.

Omi, T., Ogata, Y., Hirata, Y., & Aihara, K. (2015). Intermediate-term forecasting of aftershocks from an early aftershock sequence: Bayesian and ensemble forecasting approaches. *Journal of Geophysical Research: Solid Earth*, **120**(4), 2561-2578.

Papadimitriou, C., Beck, J. L., & Katafygiotis, L. S. (2001). Updating robust reliability using structural test data. *Probabilistic engineering mechanics*, **16**(2), 103-113.

Papadopoulos, A. N., Bazzurro, P., & Marzocchi, W. (2021). Exploring probabilistic seismic risk assessment accounting for seismicity clustering and damage accumulation: Part I. Hazard analysis. *Earthquake Spectra*, 37(2), 803-826.

Papaioannou, C. A., & Papazachos, B. C. (2000). Time-independent and time-dependent seismic hazard in Greece based on seismogenic sources. *Bulletin of the Seismological Society of America*, **90**(1), 22-33.

Roeloffs, E., & Goltz, J. (2017). The California earthquake advisory plan: A history. *Seismological Research Letters*, **88**(3), 784-797.

Segou, M. (2016). Physics-based and statistical earthquake forecasting in a continental rift zone: the case study of Corinth Gulf (Greece). *Geophysical Journal International*, *204*(1), 591-605.

Segou, M., Voulgaris, N., & Makropoulos, K. (2010). On the sensitivity of ground motion prediction equations in Greece. *Bulletin of the Geological Society of Greece*, **43**(4), 2163-2173.

Skarlatoudis, A. A., Papazachos, C. B., Margaris, B. N., Ventouzi, C., Kalogeras, I., & EGELADOS Group. (2013). Ground-motion prediction equations of intermediate-depth earthquakes in the Hellenic arc, southern Aegean subduction area. *Bulletin of the Seismological Society of America*, **103**(3), 1952-1968.

Telesca, L., Cuomo, V., Lapenna, V., Vallianatos, F., & Drakatos, G. (2001). Analysis of the temporal properties of Greek aftershock sequences. *Tectonophysics*, **341**(1-4), 163-178.

Tsapanos, T. M. (2008). Seismicity and seismic hazard assessment in Greece. In *Earthquake monitoring and seismic hazard mitigation in Balkan countries* (pp. 253-270). Springer, Dordrecht.

Utsu, T. and Ogata, Y. 1995. The Centenary of the Omori Formula for a Decay Law of Aftershock Activity. *Journal of Physics of the Earth*, **43**(1): 1–33.

Utsu, T. (1961). A statistical study on the occurrence of aftershocks. *Geophys. Mag.*, **30**, 521-605.

Vamvakaris, D. A., Papazachos, C. B., Papaioannou, C. A., Scordilis, E. M., & Karakaisis, G. F. (2016). A detailed seismic zonation model for shallow earthquakes in the broader Aegean area. *Natural Hazards and Earth System Sciences*, **16**(1), 55-84.

Wiemer, S. (2001). A software package to analyse seismicity: ZMAP. *Seismological Research Letters*, **72**(3), 373-382.

Woessner, J., Laurentiu, D., Giardini, D., Crowley, H., Cotton, F., Grünthal, G., ... & Stucchi, M. (2015). The 2013 European seismic hazard model: key components and results. *Bulletin of Earthquake Engineering*, **13**(12), 3553-3596.

Zechar, J. D., Gerstenberger, M. C., Rhoades, D. A. (2010). Likelihood-based tests for evaluating space–rate–magnitude earthquake forecasts. *Bulletin of the Seismological Society of America* **100**(3):1184-1195.

Zhang, X., & Shcherbakov, R. (2016). Power-law rheology controls aftershock triggering and decay. *Scientific reports*, **6**(1), 1-9.

Zhao, J. X., Zhang, J., Asano, A., Ohno, Y., Oouchi, T., Takahashi, T., ... & Fukushima, Y. (2006). Attenuation relations of strong ground motion in Japan using site classification based on predominant period. *Bulletin of the Seismological Society of America*, **96**(3), 898-913.

Zhuang, J. (2011). Next-day earthquake forecasts for the Japan region generated by the ETAS model. *Earth, planets and space*, 63(3), 207-216.

Zhuang, J., Werner, M. J., Hainzl, S., Harte, D., Zhou, S. (2011). *Basic models of seismicity: spatiotemporal models*. Community Online Resource for Statistical Seismicity Analysis, doi:10.5078/corssa-07487583.

APPENDIX 1

Sampling θ from the distribution $p(\boldsymbol{\theta}|\mathbf{seq},M_l)$

The probability distribution $p(\boldsymbol{\theta}|\mathbf{seq},M_l)$ in Equation (3) can be calculated using Bayesian parameter estimation as follows (see also Ebrahimian and Jalayer 2017):

$$p(\boldsymbol{\theta}|\mathbf{seq},M_l) = C^{-1}p(\mathbf{seq}|\boldsymbol{\theta},M_l)\cdot p(\boldsymbol{\theta}|M_l) \qquad \text{(Eq. A1)}$$

where $p(\mathbf{seq}|\boldsymbol{\theta},M_l)$ denotes the likelihood of the observed sequence given the vector of model parameters $\boldsymbol{\theta}$ and lower cut-off magnitude M_l, $p(\boldsymbol{\theta}|M_l)$) is the prior distribution for the vector $\boldsymbol{\theta}$, and the term C^{-1} is a normalizing constant. In lieu of additional information (e.g., statistics of regional model parameters), the prior joint distribution $p(\boldsymbol{\theta}|M_l)$ can be estimated as the product of marginal uniform probability distributions for each model parameter. The calculation of the likelihood $p(\mathbf{seq}|\boldsymbol{\theta},M_l)$ is discussed in detail in Ebrahimian and Jalayer (2017).

In order to sample from $p(\boldsymbol{\theta}|\mathbf{seq},M_l)$, a MCMC simulation routine is employed, which is particularly useful for cases where the sampling needs to be done from a probability distribution that is known up to a constant value, that is C^{-1} herein (see Beck and Au 2002). The MCMC routine uses the Metropolis-Hastings (MH) algorithm (Metropolis et al. 1953, Hasting 1970) in order to generate samples as a Markov Chain sequence used first to sample from the target probability distribution $p(\boldsymbol{\theta}|\mathbf{seq},M_l)$, and later to estimate the robust seismicity forecasting in Equation (3) and Equation (4). The MH routine generates a Markov chain that produces a sequence of samples $[\boldsymbol{\theta}_1\rightarrow\boldsymbol{\theta}_2\rightarrow\ldots\rightarrow\boldsymbol{\theta}_n\rightarrow\ldots]$, where $\boldsymbol{\theta}_n$ represents the state of Markov Chain at nth iteration. It can be shown that the samples from the chain after the initial transient ones (the first few samples are often discarded to reduce the initial transient effect) reflect samples from the target distribution $p(\boldsymbol{\theta}|\mathbf{seq},M_l)$. To generate the $(n+1)^{\text{th}}$ sample $\boldsymbol{\theta}_{n+1}$ given that the n^{th} sample $\boldsymbol{\theta}_n$ is already known, the following procedure is performed:

(a) Generate a candidate sample $\boldsymbol{\theta}^*$ from a proposal (candidate) distribution $q(\boldsymbol{\theta}|\boldsymbol{\theta}_n)$. It is important to note that there are no specific restrictions about the choice of $q(\cdot)$ apart from the fact that it should be possible to calculate both $q(\boldsymbol{\theta}_{i+1}|\boldsymbol{\theta}_i)$ and $q(\boldsymbol{\theta}_i|\boldsymbol{\theta}_{i+1})$.

(b) Accept the candidate sample with the probability min(1,r) (where r is defined in Equation (A2) as follows) and set $\boldsymbol{\theta}_{n+1}=\boldsymbol{\theta}^*$; otherwise, $\boldsymbol{\theta}_{n+1}=\boldsymbol{\theta}_n$:

$$r = \frac{p(\boldsymbol{\theta}^*|\mathbf{seq},M_l)}{p(\boldsymbol{\theta}_n|\mathbf{seq},M_l)} \cdot \frac{q(\boldsymbol{\theta}_n|\boldsymbol{\theta}^*)}{q(\boldsymbol{\theta}^*|\boldsymbol{\theta}_n)} = \left(\frac{p(\mathbf{seq}|\boldsymbol{\theta}^*,M_l)}{p(\mathbf{seq}|\boldsymbol{\theta}_n,M_l)} \cdot \frac{p(\boldsymbol{\theta}^*|M_l)}{p(\boldsymbol{\theta}_n|M_l)}\right) \cdot \frac{q(\boldsymbol{\theta}_n|\boldsymbol{\theta}^*)}{q(\boldsymbol{\theta}^*|\boldsymbol{\theta}_n)} \quad \text{(Eq. A2)}$$

where $\frac{p(\mathbf{seq}|\boldsymbol{\theta}^*,M_l)}{p(\mathbf{seq}|\boldsymbol{\theta}_n,M_l)}$ is the likelihood ratio; $\frac{p(\boldsymbol{\theta}^*|M_l)}{p(\boldsymbol{\theta}_n|M_l)}$ is the prior ratio; $\frac{q(\boldsymbol{\theta}_n|\boldsymbol{\theta}^*)}{q(\boldsymbol{\theta}^*|\boldsymbol{\theta}_n)}$ is the proposal ratio.

It can be shown, see Beck and Au (2002); Jalayer and Ebrahimian (2017), using the Total Probability Theorem that, if the current sample $\boldsymbol{\theta}_n$ is distributed as $p(\cdot|\mathbf{seq},M_l)$, the $(n+1)^{\text{th}}$ sample $\boldsymbol{\theta}_{n+1}$ is also distributed as $p(\cdot|\mathbf{seq},M_l)$. In order to improve the rate of convergence of the simulation process, we have used an adaptive MH algorithm, as proposed by Beck and Au (2002), that introduces a sequence of intermediate evolutionary candidate PDF's that resemble more and more the target PDF.

APPENDIX 2- LIST OF SYMBOLS

Symbol	**Meaning**	**Symbol**	**Meaning**
Mw	Moment magnitude	$N_b(x,y,m\|M_l)$	a constant representing the area's background seismicity
A	Aftershock zone	$\mathbb{E}[N(x,y,m\|\mathbf{seq},M_l)]$	the average number of events in the cell centred at (x, y) with a magnitude ≥ m in the forecasting interval [T_{start}, T_{end}]
λ_{ETAS}	The conditional rate of occurrence of earthquakes	$\Omega_{\boldsymbol{\theta}}$	the domain of the model parameters
$\boldsymbol{\theta}$	Model parameters	$p(\boldsymbol{\theta}\|\mathbf{seq},M_l)$	conditional posterior

			probability density function (PDF) for $\boldsymbol{\theta}$ given the $\mathbf{seq}$ and the lower cut-off magnitude M_l
$\mathbf{seq}_t$	past events	$\mathbf{seqg}$	the events within the forecasting interval
M_l	lower cut-off magnitude	$p(\mathbf{seqg}\|\boldsymbol{\theta}, \mathbf{seq}, M_l)$	the PDF for the generated sequence **seqg** given that $\boldsymbol{\theta}$ and **seq** are known
M_c	Magnitude of completeness	'M'	Number of months before the forecast interval when applying the *incremental adaptive training algorithm*
β	related to the Gutenberg-Richter relation	'E'	arbitrary subsets of events with magnitude $\geq M_c$ when applying the *incremental adaptive training algorithm*
c and *p*	MO's Law parameter	'D'	Each 'E' subset covers at least 'D' days of the catalogue when applying the *incremental adaptive training algorithm*
d and *q*	spatial distribution of the triggered events	$\boldsymbol{\sigma}$	Standard deviation
K	calibration for each forecasting interval	$\lambda(PGA > pga)$	the annual rate of exceedance of *PGA*

			above a threshold pga
K_t	Unifies the time-dependent term over infinite time	M_{min}	The minimum magnitude in PSHA
K_R	Unifies the spatial term over infinite space	M_{max}	The maximum magnitude in PSHA
α	efficiency of an event in generating aftershock activity	$\lambda(M > M_{min})$	the annual rate of exceedance of earthquakes greater than M_{min}
[T_{start}, T_{end}]	forecasting interval	$P(PGA > pga\|m, d\{(x, y), (x_s, y_s)\})$	the conditional probability of PGA exceeding a threshold pga, given a magnitude m and a epicentral distance d at the (x,y ∈ **A**)
T_o	time of origin	$f_M(m)$	probability density function of magnitude
seq	The observation history of N_o events that took place before the forecasting interval [T_o, T_{start})	$f_{X,Y}(x, y)$	the joint probability density function of the distance distribution
$N(x, y, m\|\mathbf{seq}, M_l)$	The number of events at the centre point of a given cell centred at (x, y) with magnitude ≥ m in the forecasting interval [T_{start}, T_{end}]		